DTIC FILE COPY

2

MTL TR 89-90

AD-A214 995

AD

FAILURE ANALYSIS OF A MISSILE LOCKING HOOK FROM THE F-14 JET

VICTOR K. CHAMPAGNE, Jr. and GARY WECHSLER

MATERIALS TESTING AND EVALUATION BRANCH

September 1989

Approved for public release; distribution unlimited.

US ARMY LABORATORY COMMAND
MATERIALS TECHNOLOGY LABORATORY

U.S. ARMY MATERIALS TECHNOLOGY LABORATORY
Watertown, Massachusetts 02172-0001

89 12 04 185

UNCLASSIFIED

SECURITY CLASSIFICATION OF THIS PAGE (When Data Entered)

REPORT DOCUMENTATION PAGE

READ INSTRUCTIONS BEFORE COMPLETING FORM

1. REPORT NUMBER MTL TR 89-90	2. GOVT ACCESSION NO.	3. RECIPIENT'S CATALOG NUMBER
4. TITLE (and Subtitle) FAILURE ANALYSIS OF A MISSILE LOCKING HOOK FROM THE F-14 JET		5. TYPE OF REPORT & PERIOD COVERED Final Report 6. PERFORMING ORG. REPORT NUMBER
7. AUTHOR(s) Victor K. Champagne, Jr. and Gary Wechsler		8. CONTRACT OR GRANT NUMBER(s)
9. PERFORMING ORGANIZATION NAME AND ADDRESS U.S. Army Materials Technology Laboratory Watertown, Massachusetts 02172-0001 SLCMT-MRM		10. PROGRAM ELEMENT, PROJECT, TASK AREA & WORK UNIT NUMBERS
11. CONTROLLING OFFICE NAME AND ADDRESS U.S. Army Laboratory Command 2800 Powder Mill Road Adelphi, Maryland 20783-1145		12. REPORT DATE September 1989 13. NUMBER OF PAGES 54
14. MONITORING AGENCY NAME & ADDRESS (if different from Controlling Office)		15. SECURITY CLASS. (of this report) Unclassified 15a. DECLASSIFICATION/DOWNGRADING SCHEDULE

16. DISTRIBUTION STATEMENT (of this Report)

Approved for public release; distribution unlimited.

17. DISTRIBUTION STATEMENT (of the abstract entered in Block 20, if different from Report)

18. SUPPLEMENTARY NOTES

19. KEY WORDS (Continue on reverse side if necessary and identify by block number)

High strength steels
Fatigue (mechanics)
Missile hook
Scanning electron microscopy (SEM)
Corrosion
Failure mechanics
300M Steels

20. ABSTRACT (Continue on reverse side if necessary and identify by block number)

(SEE REVERSE SIDE)

DD FORM 1 JAN 73 1473 EDITION OF 1 NOV 65 IS OBSOLETE

UNCLASSIFIED

SECURITY CLASSIFICATION OF THIS PAGE (When Data Entered)

UNCLASSIFIED
SECURITY CLASSIFICATION OF THIS PAGE (When Data Entered)

Block No. 20

ABSTRACT

A comprehensive metallurgical examination of the missile hook was conducted at the U.S. Army Materials Technology Laboratory (MTL) to determine the probable cause of failure. The component is one of two launcher housing support points for the Sparrow Missile and is located on the F-14 jet. The missile hook failed while in service.

Chemical analysis verified that the part was fabricated from 300M steel. It was determined by metallographic examination that the microstructure was martensitic. Visual inspection and light optical microscopy of the load-bearing area showed that the surface coating "Microlube" had been completely worn away during service, allowing corrosion to take place. Extensive pitting was found on surface regions near the fracture. Further analysis of the "Microlube" coating revealed that required thickness specifications were exceeded. The machined radius where the fracture initiated was measured and found to be sharper than specified. The mechanical properties of the material compared favorably with requirements. Scanning electron microscopy (SEM) and energy dispersing spectroscopy (EDS) were used to characterize the fracture surface and the surface coatings. The entire manufacturing history of the missile hook was reviewed and the service conditions were analyzed. Finally, a mechanics analysis was conducted in order to calculate the operating stresses, the critical crack size, and the critical stress intensity factor (K_{IC}) for the conditions observed. The failure was attributed to a fatigue crack that had initiated at the base of an undercut radius on the machined lip of the component.

UNCLASSIFIED
SECURITY CLASSIFICATION OF THIS PAGE (When Data Entered)

CONTENTS

BACKGROUND

The missile hook (Figure 1a) is located on the F-14 jet and is part of the Lau 92 Ejection Launcher System. The component is one of two launcher housing support points for the Sparrow Missile, as shown in Figure 1b.

The missile hook failed in August, 1987, after approximately 8 years and 10 months of service. Failure occurred as an F-14 landed on an aircraft carrier. A total of four parts have failed in service since 1981, see Table 1.

Table 1. MISSILE HOOK FAILURES

NHA Serial No.	Date of Failure	Age of Component	Cause of Failure
CSS-099	November 1981	8 yr/9 mo	Fatigue Due to Undercut Radius
CSS-141	October 1983	11 yr/5 mo	Part was Lost
HJR-166	November 1983	5 yr/11 mo	Ductile Overload at the Radius
JCU-076*	August 1987	8 yr/10 mo	Ductile Overload Caused by Fatigue Crack at Undercut Radius

*Denotes the part under investigation

VISUAL INSPECTION/LIGHT OPTICAL MICROSCOPY

Figure 2 shows the area of concern on the missile hook, at low magnification. The failure occurred along the lower radius of the machined lip. Radial marks were easily distinguishable on the fracture faces. These lines resulted from the intersection and connection of fractures propagating at different levels. The crack initiation site was identified when these lines were traced back to the point of convergence (refer to Zone 1). Some of the outside edges of the fracture faces contained shear lip zones which were characterized by their gray, silky appearance. At the crack origin, a typical "thumbnail" crack could be seen extending outward (refer to Zone 1) which suggested that an older crack may have existed before final, fast fracture occurred. This was later verified by further examination.

Another notable feature of the fracture surface was an area that resembled a "quarter moon" (refer to Zone 3). Scanning electron microscopy (SEM) was utilized to obtain additional metallurgical information from this region as well as the remaining fracture surface. These results are included as part of the fractographic analysis of this report. Fracture Face 2 appeared to have less corrosion and surface debris than Fracture Face 1. It was later discovered that Fracture Face 2 was recovered from the deck of the aircraft carrier after the failure occurred and placed in storage, protecting it from the elements. Fracture Face 1, however, was still attached to the aircraft and was removed at a much later date. The salt water environment caused additional corrosion to take place on the unprotected fracture surface.

The hook is inserted into a mating component, located on the 500 lb Sparrow Missile (Figure 1b) providing support and stability. The contact areas between these parts are subjected to vibration and shock loading during all phases of flight, especially while landing the aircraft. This repeated motion caused mechanical wear at the interface.

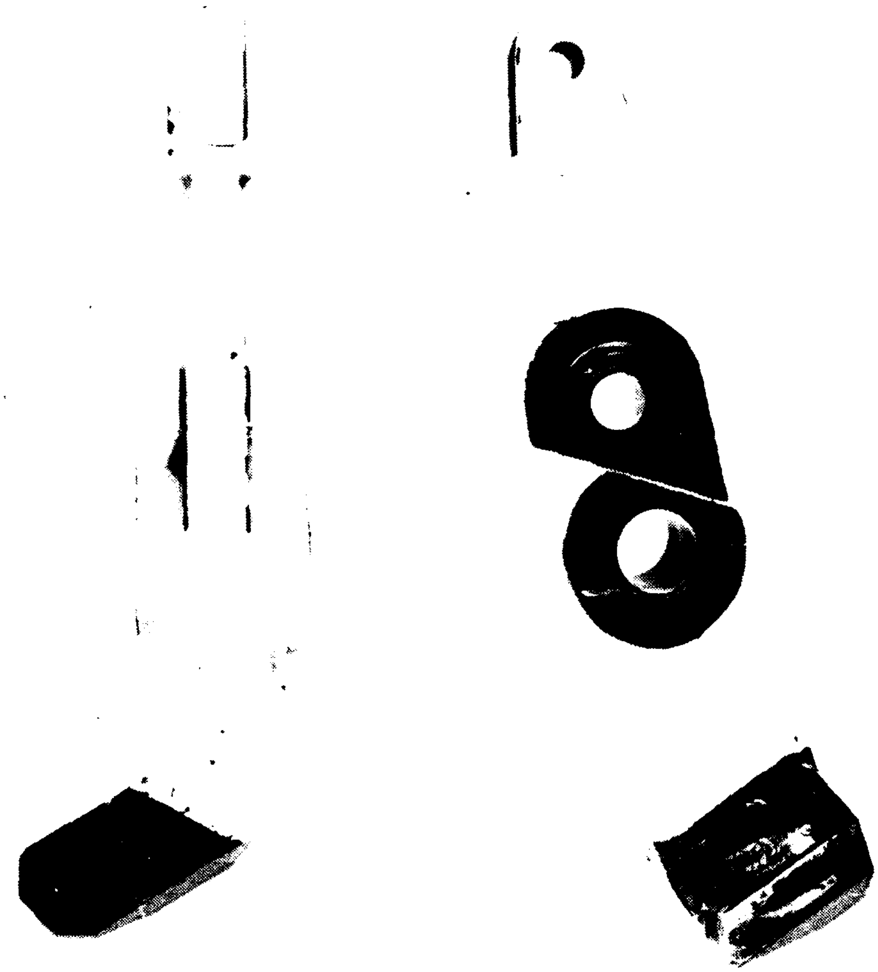

Figure 1a. Reduced photographs revealing two views of the missile hook.

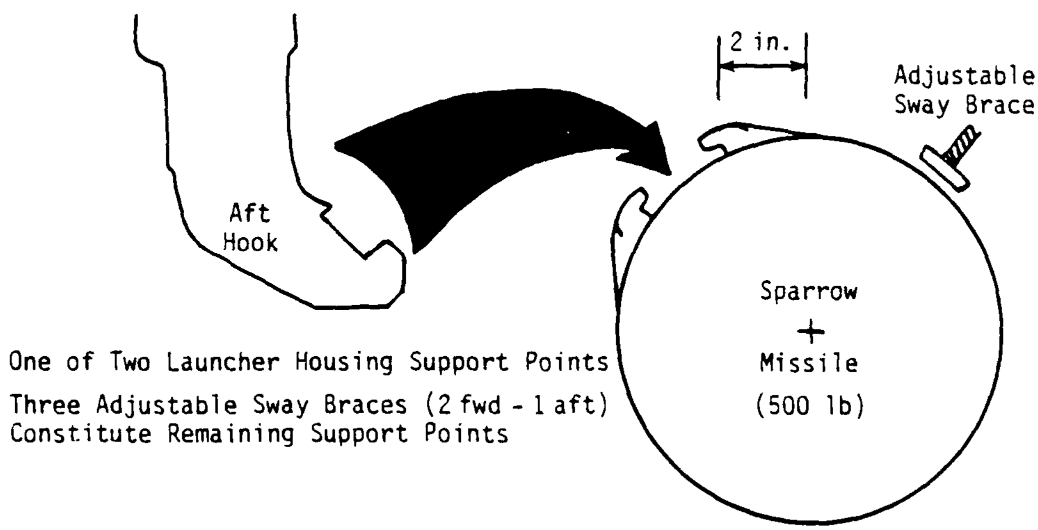

Figure 1b. Schematic illustrating the locations of the support points on the Sparrow Missile.

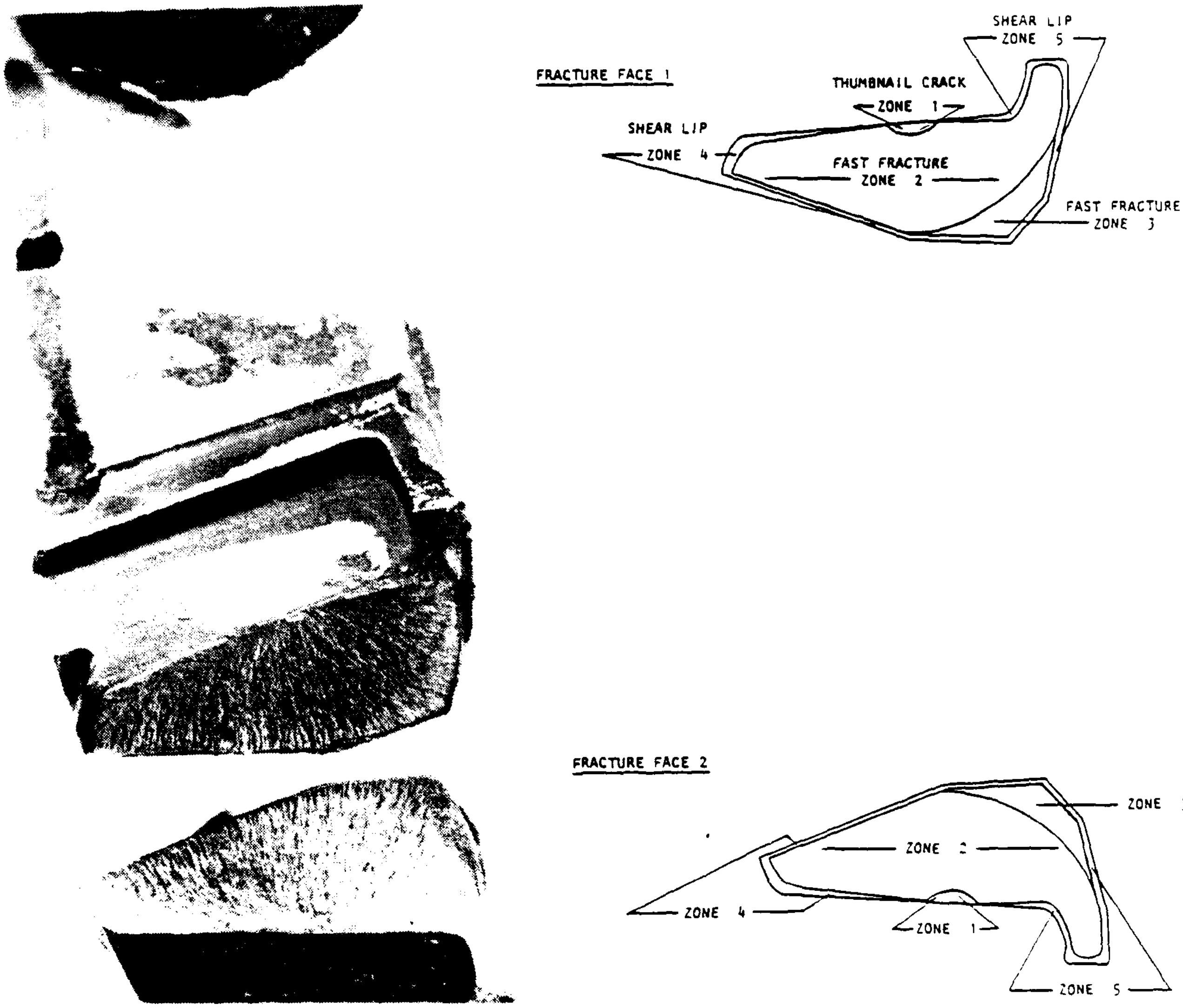

Figure 2. Macrograph of the failed missile hook showing the fracture faces. The schematic to the right identifies different regions of the fracture which were examined.

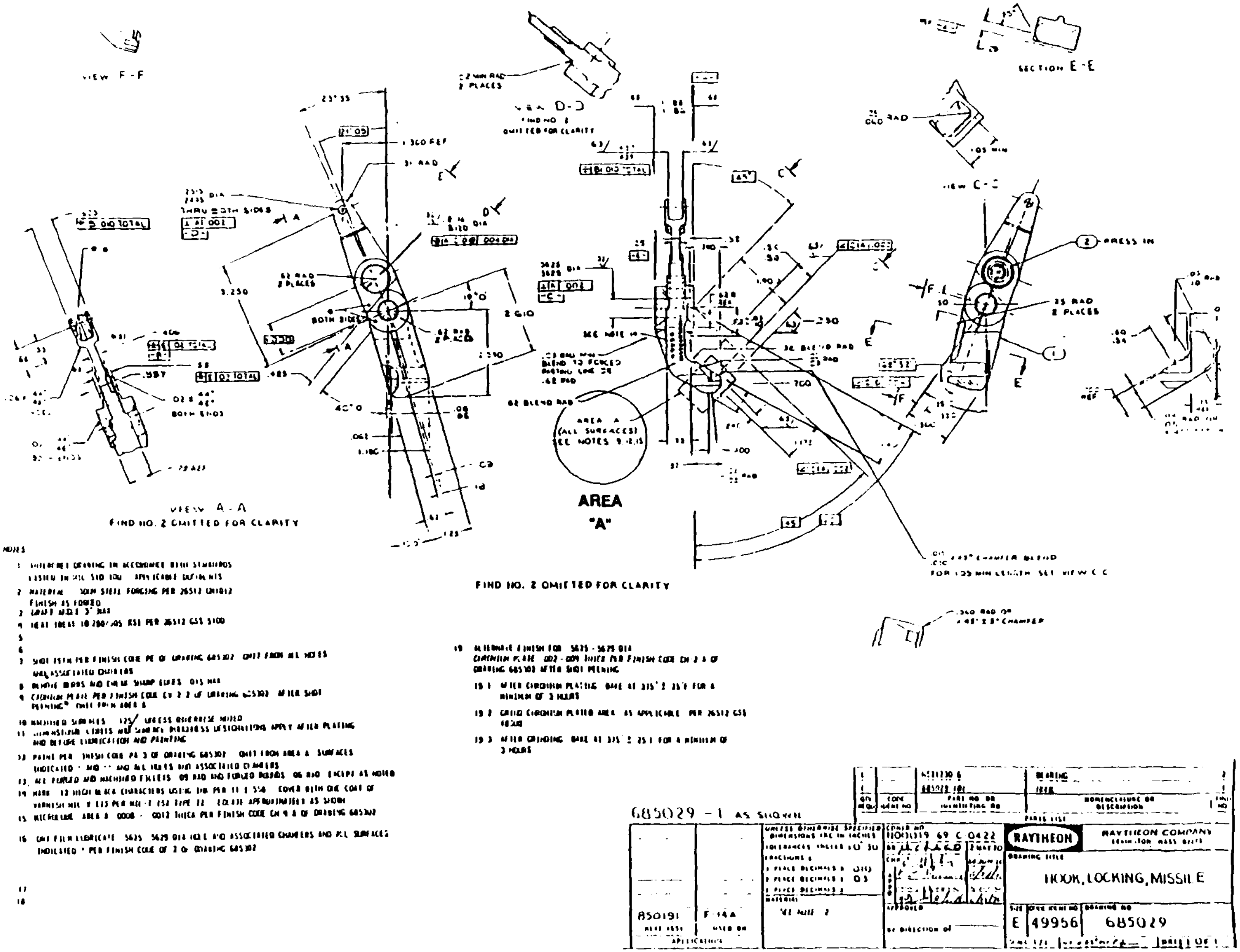

Figure 3. Engineering drawing of the missile hook.

The black "Microlube" coating located on the entire surface of Area "A" (refer to Figure 3) was inspected. The coating was badly damaged along the machined surface near the fracture line. In many regions, it had been completely worn away by abrasion. A series of macrographs were taken of several locations near the fracture, which represented the condition of the "Microlube" coating that was still intact (see Figure 4).

Figure 4. Macrograph showing three different areas where the coating had blistered and peeled away from the substrate, Mag. 25X.

Further examination of surfaces near the fracture, where the "Microlube" coating had been completely abraded away, revealed evidence of corrosion. Localized attack occurred here because of the absence of a protective coating (see Figures 5 and 6).

Figure 5. Macrograph of the surface near the crack initiation site on Fracture Face 1 showing localized corrosion attack, Mag. 20X.

Figure 6. Macrograph of the surface near the crack origin on Fracture Face 2 revealing extensive pitting, Mag. 15X.

RADIUS EXAMINATION

The upper radius of the machined lip, as shown in Figure 7, was measured and found to be approximately 0.015. The engineering drawing of the missile hook, as depicted in Figure 3, specified a radius of 0.02 to 0.03. This measurement might serve as an indication that the lower radius was also machined slightly sharper than specifications allowed, since both radii are continuations of each other, having the same specified measurements and tolerance ranges. The lower radius, where the fracture originated, could not be measured accurately because the material had been deformed in this area as a result of the failure.

Another notable feature of the radius along the machined lip was the fact that it was undercut, as revealed in Figure 7. The schematic located adjacent to Figure 7 illustrates this point. An undercut radius reduces the cross-sectional area of the load-bearing region, decreasing its strength. A sharp radius will serve as a stress concentration area and have a detrimental effect on the fatigue life of the component.

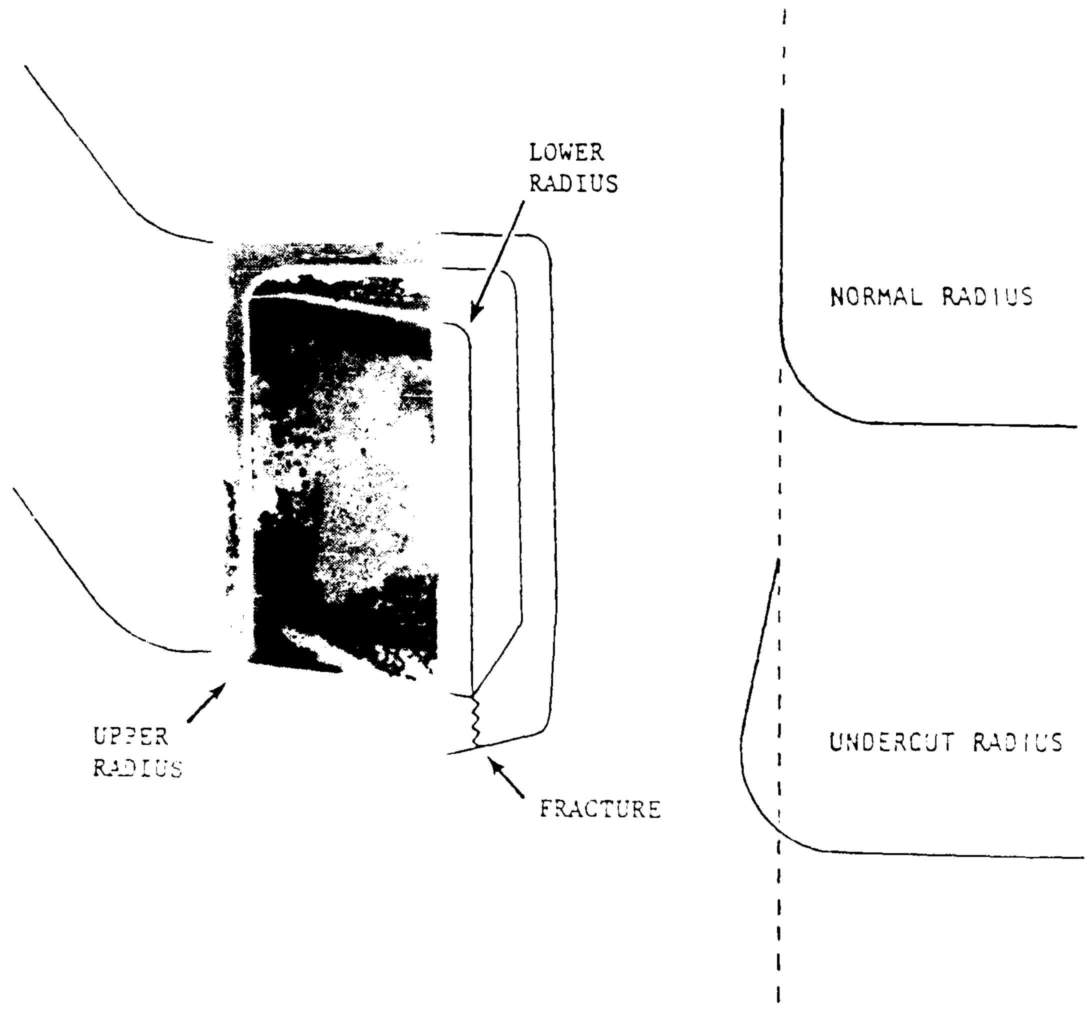

Figure 7 Macrograph showing the undercut radius of the missile hook, Mag. 3X

MICROSTRUCTURE

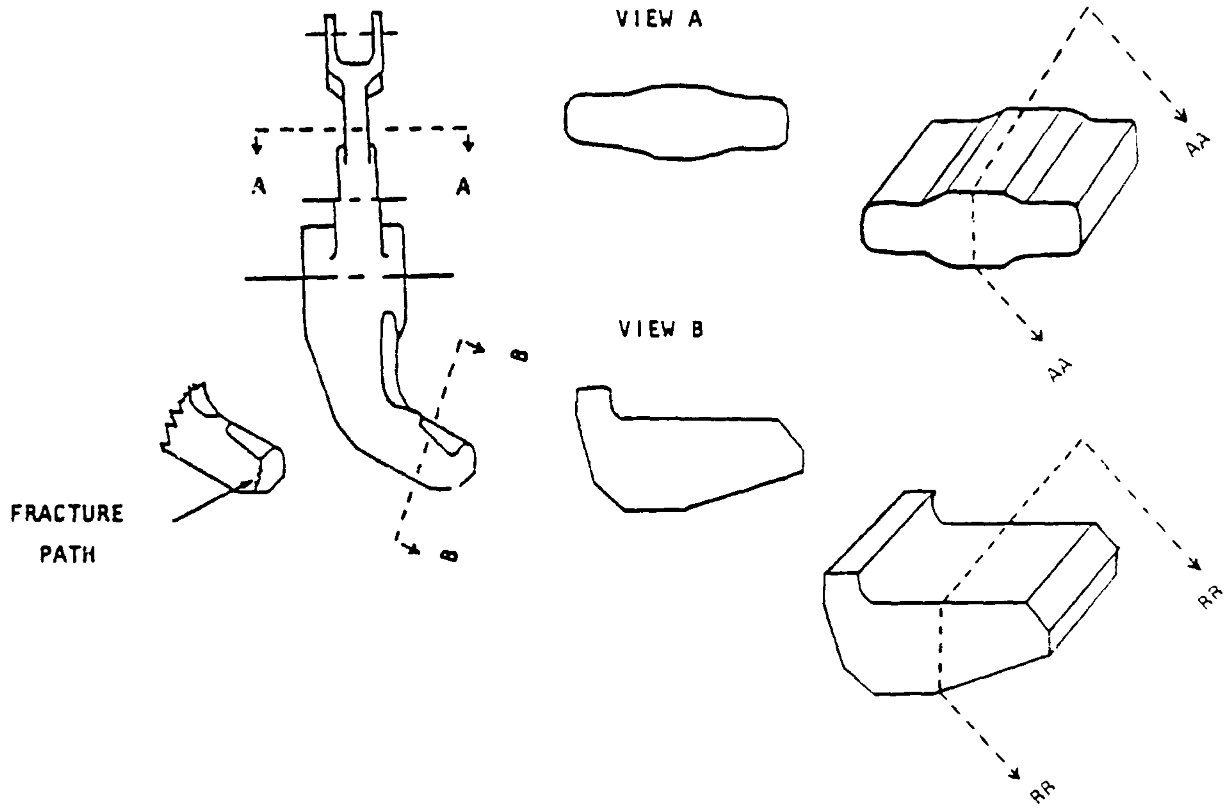

Figure 8. Schematic illustrating the areas where metallographic specimens were sectioned from the missile hook.

According to the specifications, the part is cadmium plated by vacuum deposition, per MIL-C-8837, to 0.0003 inch thick and primed, per MIL-P-23377, to 0.0006 to 0.0009 inch thick and subsequently painted with polyurethane, per MIL-C-81773, or with an acrylic lacquer, per MIL-L-81352, with the exception of the load-bearing area near the lip which is "Microlubed" to 0.0008 to 0.0012 inch thick. The "Microlube" coating is a proprietary process which includes deposition of a chromium-based alloy by ion displacement in a prescribed matrix followed by a duplex electro registration of a fluorocarbon polymer as a friction and corrosion inhibitor within the prescribed matrix. Specimens A and AA obtained from the component, as shown in Figure 8, will be used for analysis of the cadmium plating and the paint. Specimens B and BB will be utilized for examination of the "Microlube" coating.

The transverse and longitudinal sections were polished and etched to reveal the microstructural features of the material. A Nital etchant revealed a typical tempered martensitic structure in all instances, as shown in Figures 9 and 10. Close examination of the microstructure at the crack initiation site, and at areas adjacent to the fracture, was conducted in order to detect any possible structural changes which may have occurred during fabrication or in service. There were no signs of grain refinement nor any areas found that contained unusual precipitation and coagulation of carbides which may have been present if the material had been locally heated as a result of excessive grinding or rubbing. Also, no large inclusions were found in any of the specimens examined.

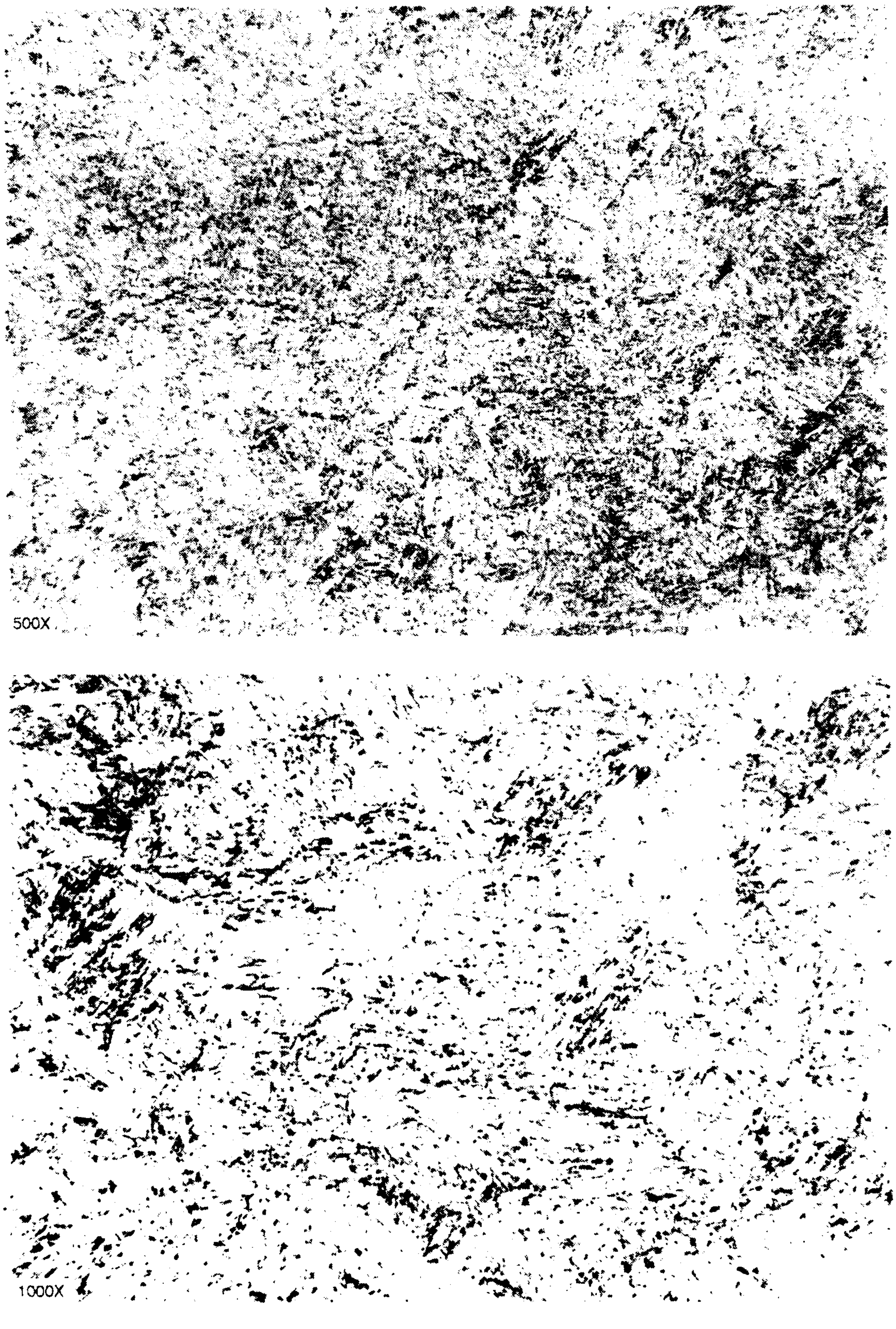

(a)

(b)

Figure 9. Micrographs of longitudinal sections showing a tempered martensitic structure.

(a)

(b)

Figure 10. Micrographs of transverse sections. The material is clean with no evidence of any major inclusions.

CORROSION ATTACK

The material under investigation (300M steel) is susceptible to hydrogen embrittlement when heat treated to strength levels greater than 200 ksi.[1] The missile hook had a measured hardness range of HRC 56 to 58 which translates to an ultimate tensile strength of approximately 284 to 299 ksi. Consequently, concern was expressed over the extent of pitting that occured near the crack origin, since the corrosion process can be a source of atomic hydrogen. In a corrosion cell, hydrogen ions can be reduced, producing hydrogen atoms and the subsequent formation of hydrogen molecules. If a sufficient amount of nascent hydrogen migrated into the steel, it could become embrittled and subject to premature cracking. Figure 11 shows regions adjacent to the fracture that contained pitting. The measured depth of attack on these specimens ranges from approximately 0.001 to 0.005 inches.

(a)

(b)

Figure 11. Macrographs of transverse cross sections taken prior to polishing that show pitting, Mag. 60X.

1. *Heat Treating of Steel.* ASM Metals Handbook, Heat Treating, v. 4, 1981, p. 122.

Pitting may also be detrimental to the useful service life of the component because the root of a pit is an area of high stress concentration where a fatigue crack could initiate and propagate. Figures 12 through 14 show transverse cross-sectional views of specimens in the as-polished condition that contained pits.

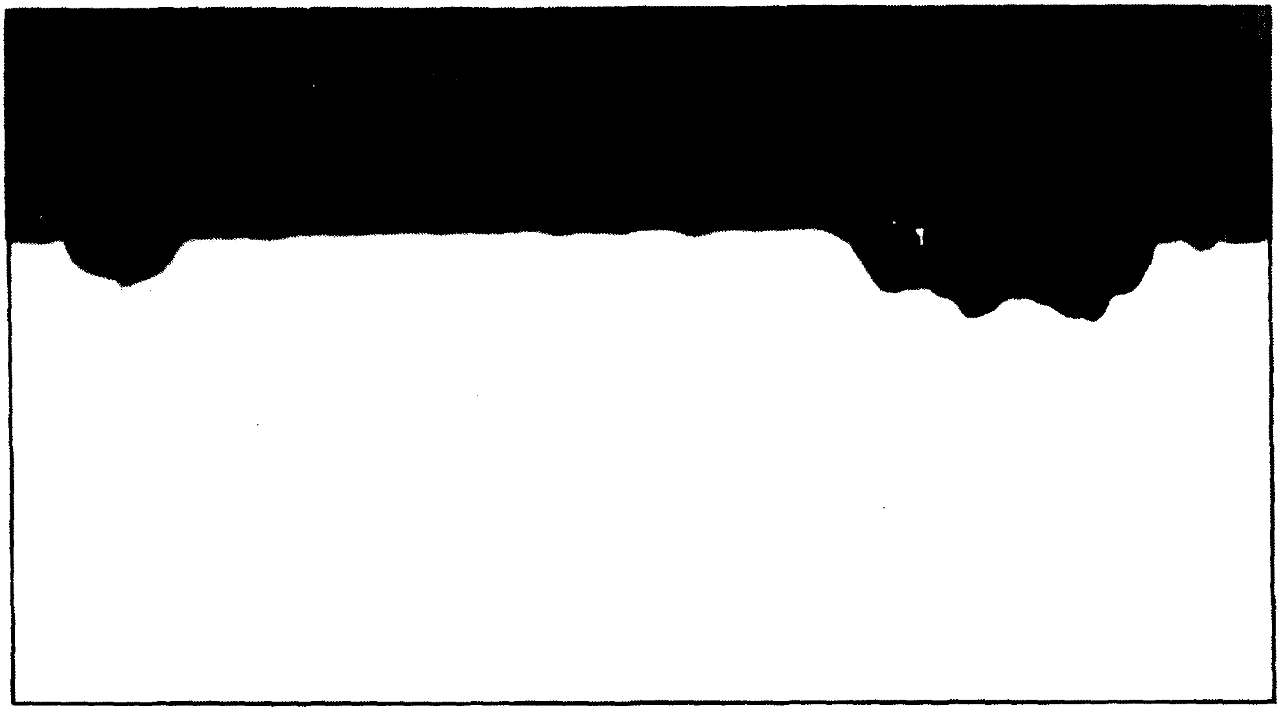

Figure 12. Micrograph revealing evidence of pitting attack. Pit depth is 0.002 to 0.005 inches, Mag. 100X.

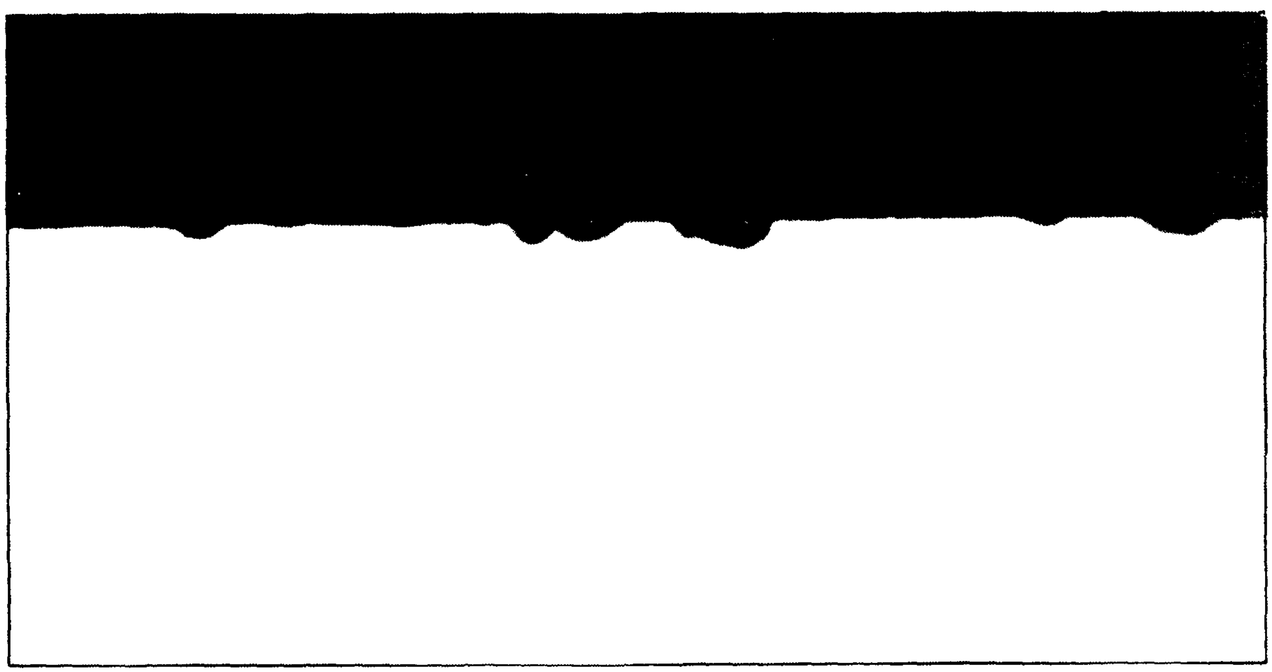

Figure 13. Micrograph showing a number of isolated pits. Maximum pit depth is 0.002 inches, Mag. 100X.

The amount of pitting found on the surface near the fracture varied. Some areas contained pits that were isolated, as shown in Figure 13. Other regions developed pits that were so close together that they resembled a rough surface, as seen in Figure 14.

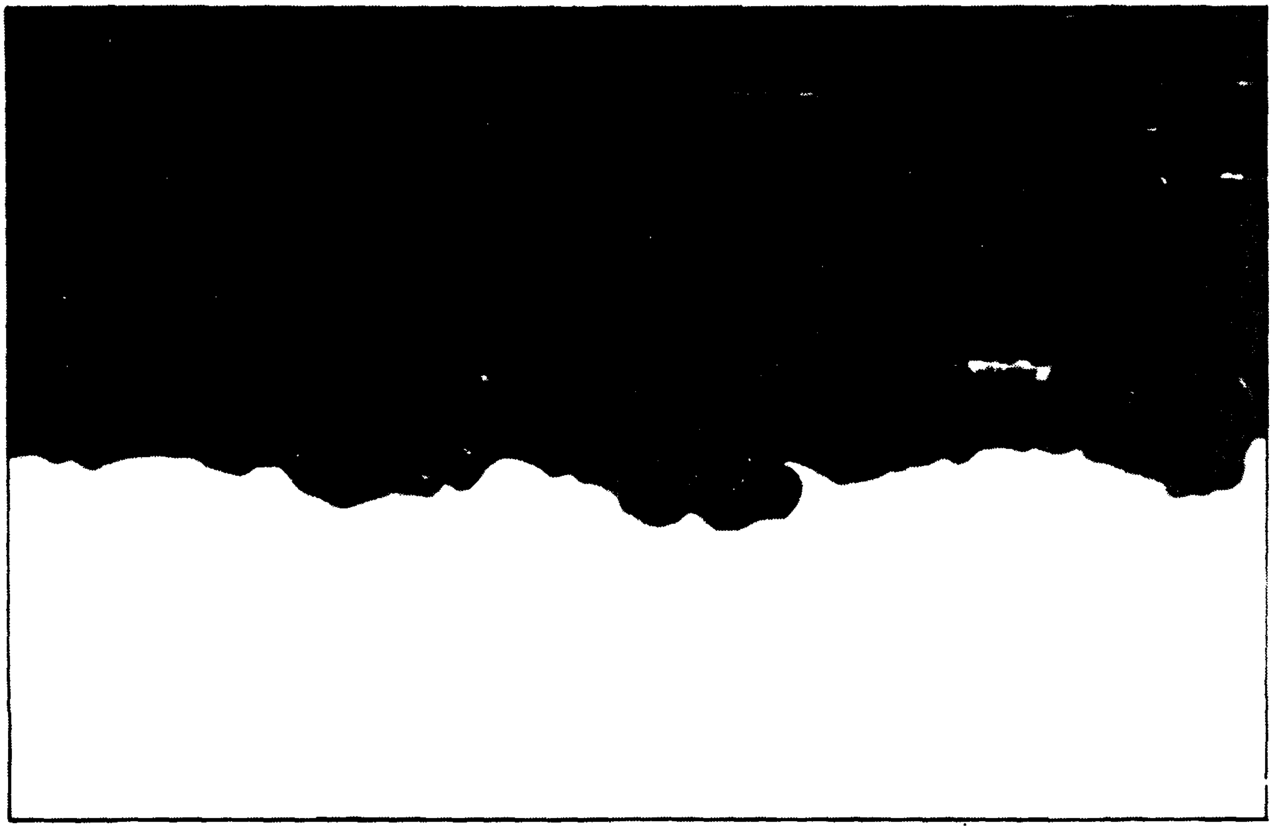

Figure 14. Micrograph of a region which contains extensive pitting damage, Mag. 100X.

CHEMICAL ANALYSIS

The missile hook is required to be fabricated from 300M steel (reference Raytheon Drawing No. 685029, Figure 3). Atomic absorption and inductively coupled argon plasma emission spectroscopy were used to determine the chemical composition of the alloy. The carbon and sulphur content was analyzed by the LECO combustion method. Typical ranges for this material, taken from the American Society for Metals Handbook and from MIL-S-8844D, have been included for comparative purposes. The compositional ranges of the material under investigation compared favorably with published values, see Table 2.

Table 2. COMPARISON OF CHEMISTRIES

Element	C	S	Mn	Si	Cr	Ni	Mo	V	P
Missile Hook	0.39	0.001	0.81	1.54	0.79	1.74	0.40	0.08	0.007
ASM Handbook*	0.40-0.46	—	0.65-0.90	1.45-1.80	0.70-0.95	1.65-2.00	0.30-0.45	0.05 Min.	
MIL-S-8844D†	0.40-0.45	0.010 Max.	0.65-0.90	1.45-1.80	0.70-0.95	1.65-2.00	0.35-0.45	0.05 Min.	0.010 Max.

*Reference 2
†Reference 3

2. *Heat Treating of Steel.* ASM Metals Handbook, Heat Treating, v. 4, p. 120.
3. MIL-S-8844D. *Steel Bar, Reforging Stock and Mechanical Tubing, Low Alloy, Premium Quality.* Table II Chemical Composition. June 1987, p. 12.

HARDNESS TESTING

Table 3. MACROHARDNESS MEASUREMENTS
VICKERS (DPH)
500g LOAD

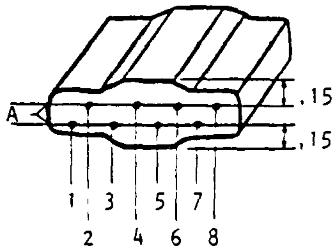

Sample A

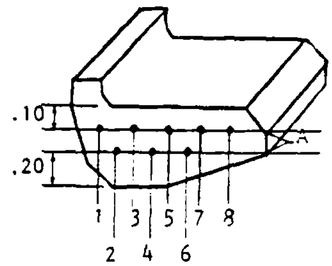

Sample B

Sample A No. Readings	Distance From Edge of Sample A Starting at Point A (in.)	Hardness DPH	Tensile Strength* (ksi)	Sample B No. Readings	Distance From Edge of Sample B Starting at Point A (in.)	Hardness DPH	Tensile Strength* (ksi)
1	0.15	586	296	1	0.15	573	290
2	0.25	555	280	2	0.25	554	278
3	0.35	560	283	3	0.35	574	290
4	0.45	568	287	4	0.45	563	285
5	0.55	560	283	5	0.55	572	289
6	0.65	563	285	6	0.65	586	296
7	0.75	579	293	7	0.75	584	295
8	0.85	552	277	8	0.85	550	276
	Average	565	286		Average	570	288

*Reference 4

Macrohardness measurements were taken along transverse cross sections of the missile hook and are listed in Table 3. Sample A was representative of the hardness measured across the upper regions of the component. Sample B was taken adjacent to the fracture at the lower end of the missile hook. The Vickers hardness values were extrapolated and converted to tensile strength for convenience in comparison. These approximate values compared favorably with the specified strength requirements of 280 to 305 ksi (refer to Raytheon Drawing No. 685029, Figure 3). The tests did not reveal evidence of any regions which displayed relatively higher or lower degrees of hardness.

4. ASM Metals Handbook, Desk Edition, Glossary of Metallurgical Terms and Engineering Tables, 1985, p. 1-60.

Table 4. MICROHARDNESS MEASUREMENTS
KNOOP HARDNESS
20x-500g LOAD
DIAMOND PENETRATOR

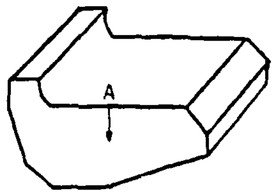

Sample A

Sample A No. Readings	Distance From Edge of Sample Starting at Point A (in.)	Hardness Knoop	Tensile Strength* (ksi)	Sample A No. Readings	Distance From Edge of Sample Starting at Point A (in.)	Hardness Knoop	Tensile Strength* (ksi)
1	0.004	584	277	14	0.034	591	281
2	0.006	588	279	15	0.038	577	273
3	0.008	605	288	16	0.050	591	281
4	0.010	589	279	17	0.070	560	265
5	0.012	627	299	18	0.090	578	273
6	0.014	596	284	19	0.110	587	279
7	0.016	616	294	20	0.130	591	281
8	0.018	609	290	21	0.150	555	262
9	0.020	601	287	22	0.170	586	278
10	0.022	590	280	23	0.190	562	265
11	0.024	628	299	24	0.210	588	279
12	0.026	582	276	25	0.230	589	279
13	0.030	587	279	26	0.250	602	287
					Average	591	281

*Reference 4

Microhardness measurements were taken starting from the surface of a transverse cross section of an area adjacent to the fracture and leading toward the interior of the component in a transverse direction, see Table 4. This procedure was conducted to verify the results obtained from metallographic examination of this same region. The Knoop hardness values were extrapolated and converted to tensile strength for comparison to specified requirements. There was no indication of possible grain refinement or any areas that contained unusually higher or lower degrees of hardness.

FRACTOGRAPHY

The fracture faces of the component were examined at higher magnifications utilizing the SEM in order to identify the failure mode in each of the distinct fracture zones shown schematically in Figure 2. Figure 15 contains a macrograph of Fracture Face 2 obtained by light optical microscopy, while Figure 16 is a SEM fractograph taken of the same region. The crack initiation site was determined by tracing the radial marks indicative of crack growth back to the point of convergence. The crack origin was contained within Zone 1, also referred to as the "thumbnail" crack region, shown in both figures. A dark layer covers this area making it easy to distinguish. The shape of this type of fracture usually suggests a single point crack origin which may occur as a result of an inclusion or a notch. However, further microscopic examination did not reveal any evidence linking the cause of failure to a corrosion pit, a surface discontinuity, or an inherent material defect.

Energy dispersing spectroscopy (EDS) of the dark material produced spectra that contained those elements associated with the type of steel under investigation as well as oxygen (see Figures 17a and 17b). The black layer was concluded to have been a corrosion product, and not contaminants. The formation of this oxide layer was later attributed as having occurred during the slow propagation of a service-related fatigue crack. Figure 15 shows a series of fine progression marks, or beach marks, barely visible within Zone 1. These macroscopic features reveal successive positions of an advancing crack front and are associated with fatigue-fracture surfaces. Under microscopic examination, fatigue striations were observed within Zone 1. Striations often occur in fatigue fractures and are the result of a single cycle of loading. Figure 18 shows these striations, which extend horizontally across the fractograph. Corrosion products are visible in various locations of the figure. Excessive corrosion can mar the fracture surface making it nearly impossible to distinguish microstructural features and interpret topology. The fracture under investigation contained a significant amount of corrosion in Zone 1, which made fractographic observations difficult in that area, but also verified that this region was the result of a preexisting crack which had been exposed to the environment for a period of time.

Corrosion was prevalent over the entire surface of the "thumbnail" crack region. In most of the locations observed with the SEM, it had inhibited conclusive fractographic interpretation of the failure mode. In areas that could be examined and characterized with some degree of certainty, Zone 1 was determined to have contained a ductile dimpled morphology, as indicated in Figure 19.

Further scanning electron microscopy was performed on the remaining fracture zones identified in Figure 2. The transitional region located between Zone 1 and Zone 2 was examined. Figure 20 is a representative SEM fractograph of that area. The surface morphology consisted of dimples with some evidence of tearing topography surface (TTS). The TTS fractures do not exhibit as much plastic deformation as a dimpled rupture, and may be the result of a microplastic tearing process.[5] Tearing topography surface is often observed along with well-defined dimples.

The surface topography of Zone 2 is represented by Figure 21. Well-developed conical equiaxed dimples indicative of microvoid coalescence can be seen in this figure. This type of fracture mode occurs under a primarily uniaxial tensile stress and is most commonly associated with an overload condition.

5. *Modes of Fracture*. ASM Metals Handbook, Fractography, v. 12, 9th ed., p. 21-22.

The area previously described as resembling a "quarter moon" was examined and labeled as Zone 3. This region was most likely the result of a brief interruption of the advancing crack fron (such as a shift or a change in loading) which later resumed its course until final rupture occurred. The single progression mark that outlines Zone 3 remains as evidence supporting this conclusion. Zone 3 also contained a conical equiaxed dimpled surface, confirming that the fracture mode was similar to that of Zone 2, as depicted in Figure 21.

The fracture regions identified as Zones 4 and 5 were determined to be shear lips. These areas were the result of a stress change to macroshear, forming fractures approximately 45° to the plane of the fracture. Figure 22 reveals the surface morphology of these shear lip regions. Dimples which are directional can be seen in this SEM fractograph.

The surfaces adjacent to the fracture were also examined utilizing the SEM. Figure 23 is representative of many of the locations observed. The absence of a protective coating in these regions allowed extensive pitting to take place. Pits act as localized stress concentration areas and may initiate a crack. Figure 24 shows an example of how a crack initiated at the root of a corrosion pit.

Subsequent to the completion of the fractographic analysis of the missile hook, an attempt was made to clean Fracture Face 1 in order to examine Zone 1 more effectively. The process involved ultrasonic cleaning of the sample in a mild detergent solution which was then followed by electrochemical cleaning in an ENDOX 214 solution.[6] This procedure is not recommended for high strength steels since it includes cathodic cleaning and, therefore, presents a risk of hydrogen embrittlement. Fracture Face 1 was chosen to undergo the process because it had suffered much more corrosion than Fracture Face 2.

Figure 24 shows Fracture Face 1 after cleaning. The dark corrosion product indicative of Zone 1 is barely visible. However, extensive cracking had occurred, after only a brief period, as a result of the cathodic reaction which was the cleaning mechanism in this process. Many of the cracks had initiated at stress concentration areas (such as corrosion pits) along the surface. Single cracks that were virtually without branches were observed while, in other instances, cracks formed in multibranched river delta patterns. Figures 25 and 26 reveal a crack that had experienced branching.

Zone 1 was significantly damaged by the effects of the corrosion process which had left behind an irreconcilable topography in most areas. However, the surface morphology was found to consist of dimples in regions that could be accurately interpreted, as previously shown in Figure 19. The cleaning procedure utilized reaffirmed the fact that the material under investigation was very susceptible to hydrogen embrittlement.

6. YUZAWICH, P. M., and HUGHES, C. W. *An Improved Technique for Removal of Oxide Scale from Fractured Surfaces of Ferrous Materials.* Practical Metallography, 1979, p. 184-194.

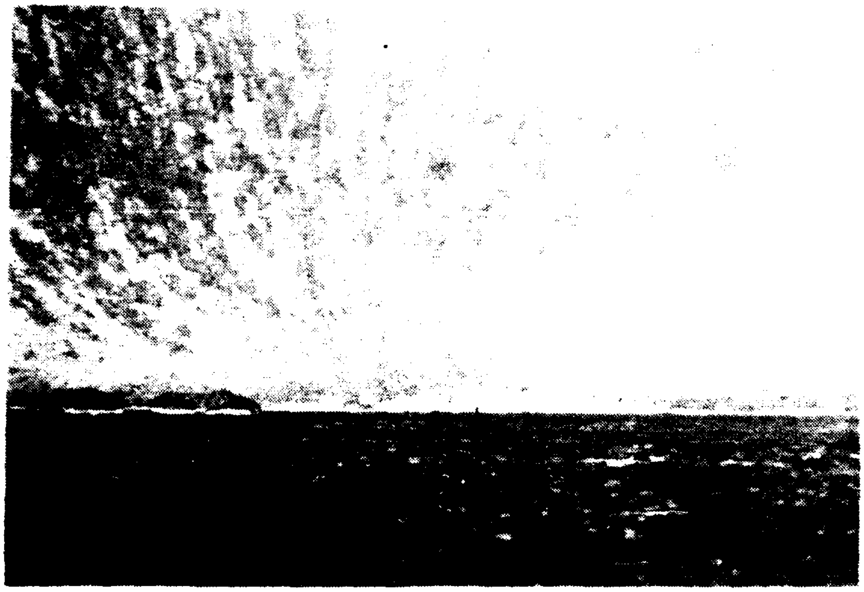

Figure 15. Optical macrograph of Fracture Face 2 revealing evidence of beach marks emanating from the crack origin in Zone 1, as identified by the arrow, Mag. 10X.

Figure 16. SEM fractograph showing the thumbnail crack area (Zone 1) and a portion of the fast fracture region (Zone 2), Mag. 10X.

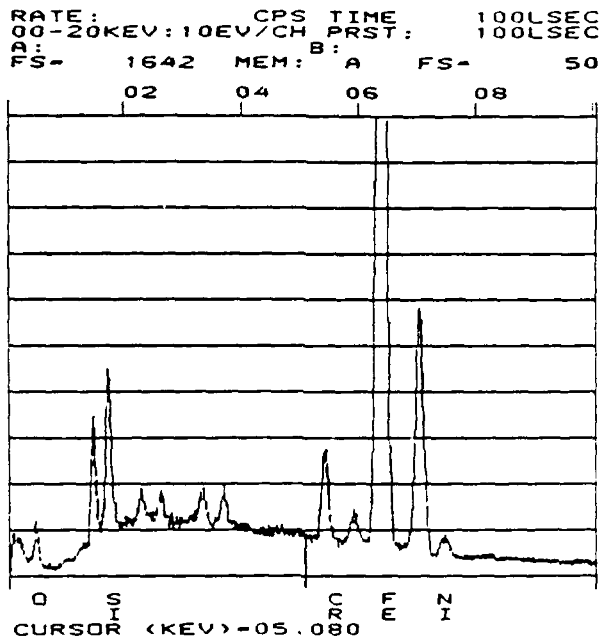

Figure 17a. EDS spectra of Zone 1 showing the elemental constituents of 300M steel and oxygen.

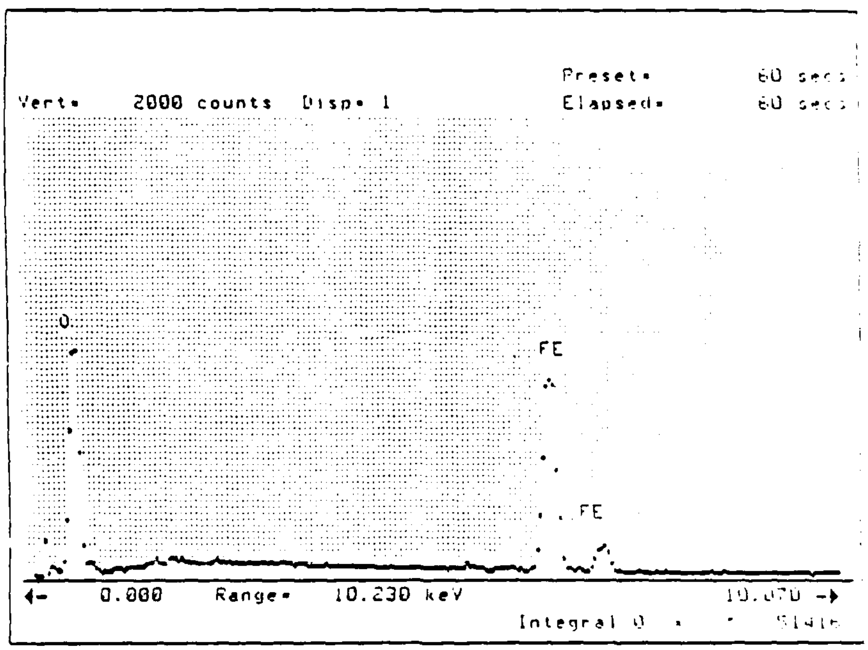

Figure 17b. EDS analysis of another region located in Zone 1 containing large amounts of iron and oxygen.

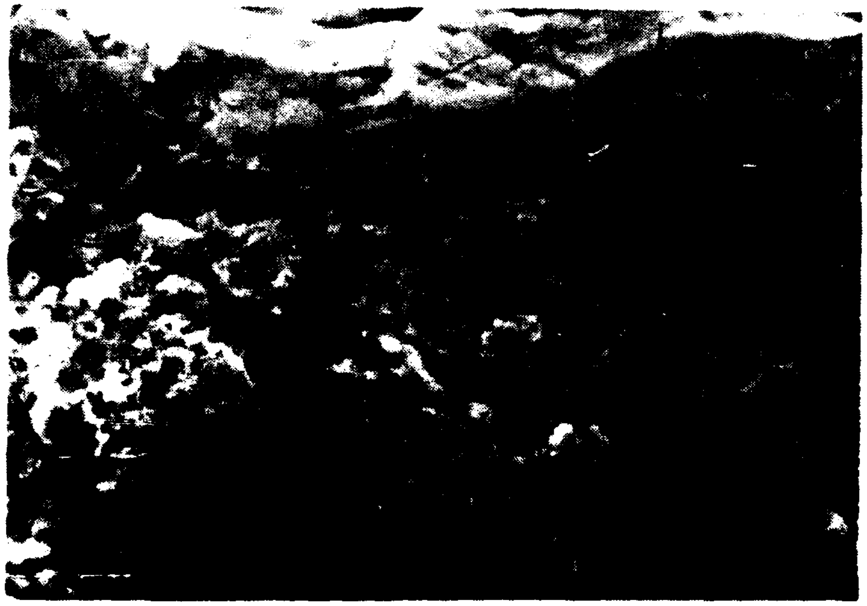

Figure 18. SEM fractograph; the arrows point out bands of closely spaced striations in Zone 1, Mag. 5000X.

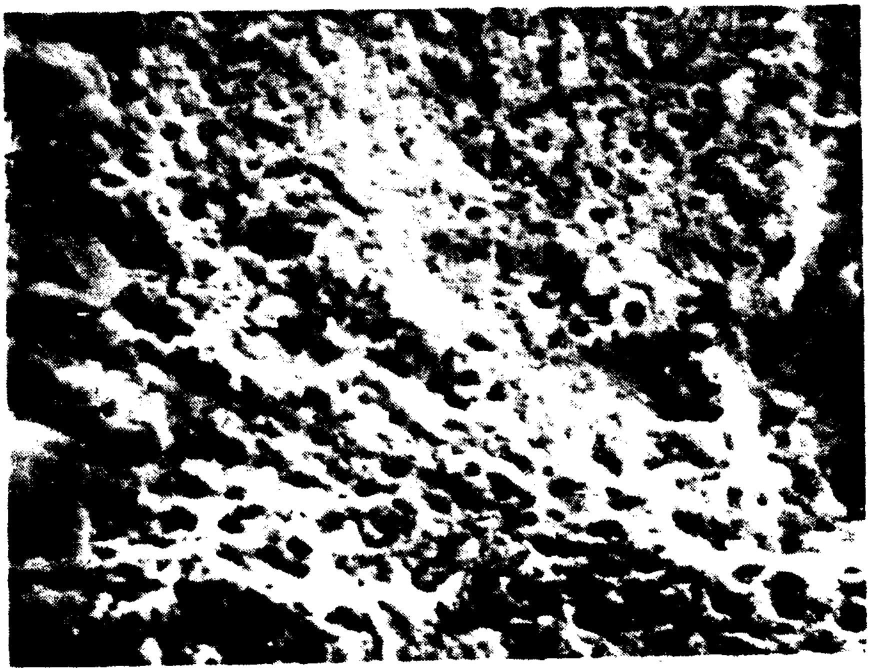

Figure 19. SEM fractograph of Zone 1 revealing a dimpled surface topography in regions that have not been obliterated by corrosion, Mag. 2000X.

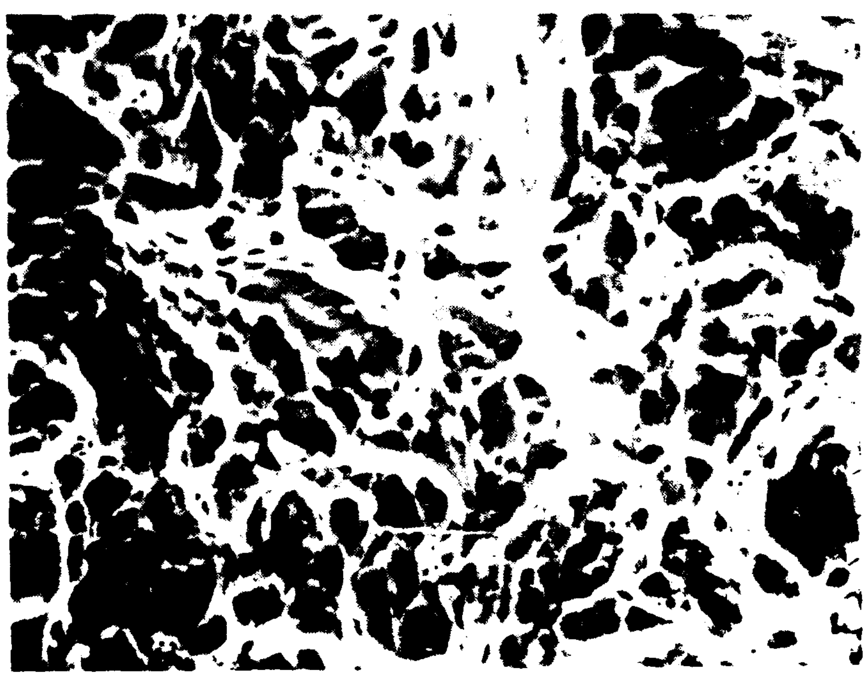

Figure 20. SEM fractograph of the transitional area between Zone 1 and Zone 2 showing evidence of tearing topography surface amidst ductile dimples, Mag. 2000X.

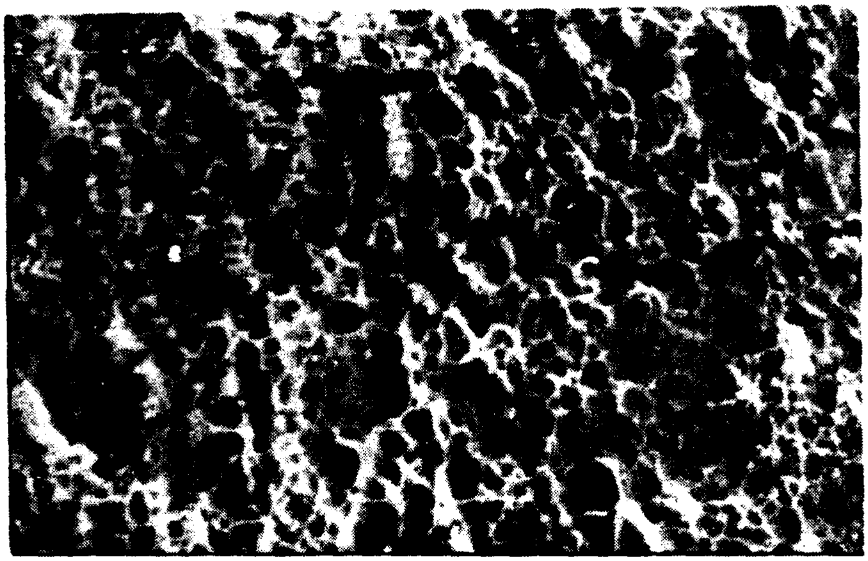

Figure 21. SEM fractograph representative of Zone 2 and Zone 3 showing a surface consisting of conical equiaxed dimples, Mag. 2000X.

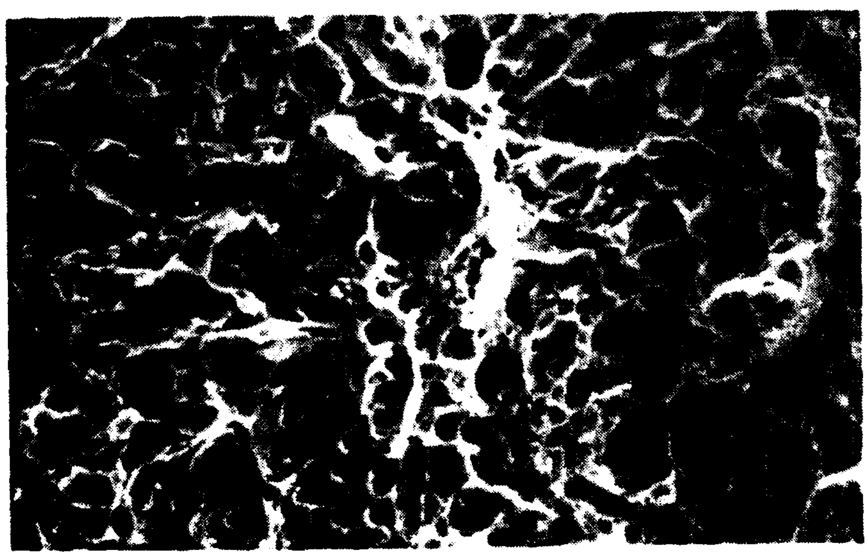

Figure 22. SEM fractograph containing slightly directional dimples indicative of Zone 4 and Zone 5, Mag. 2000X.

Figure 23. SEM micrograph of the severely pitted surface adjacent to the fracture site, Mag. 100X.

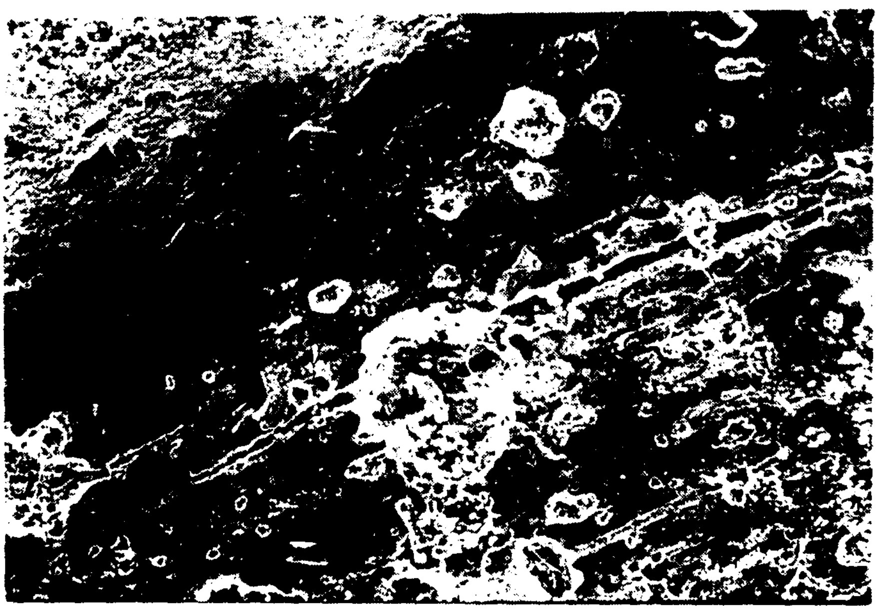

Figure 24. SEM micrograph of a crack that has initiated from the root of a corrosion pit located on the machined surface adjacent to the fracture, Mag. 250X.

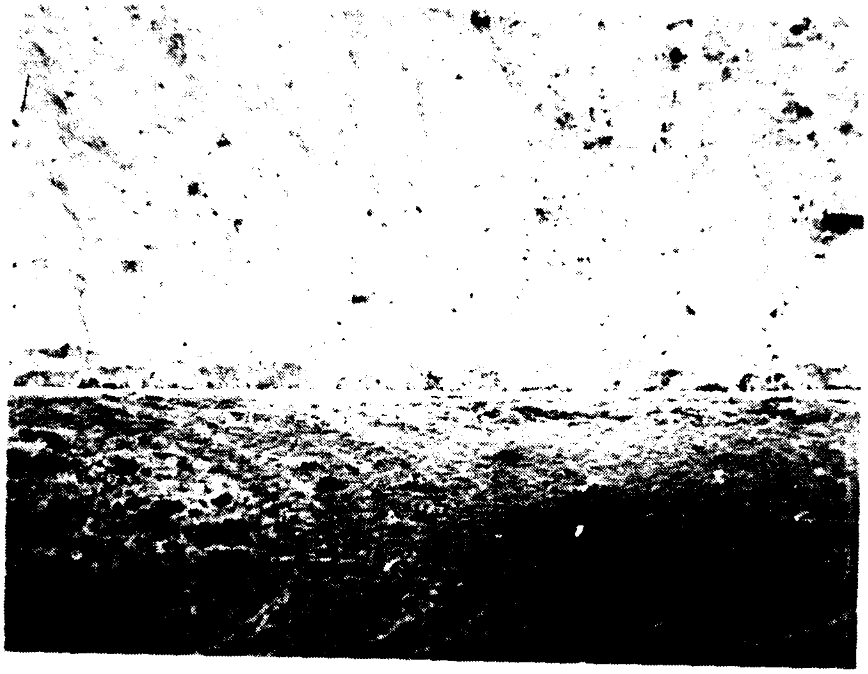

Figure 25. SEM micrograph taken after Fracture Face 1 was cathodically cleaned, Mag. 15X.

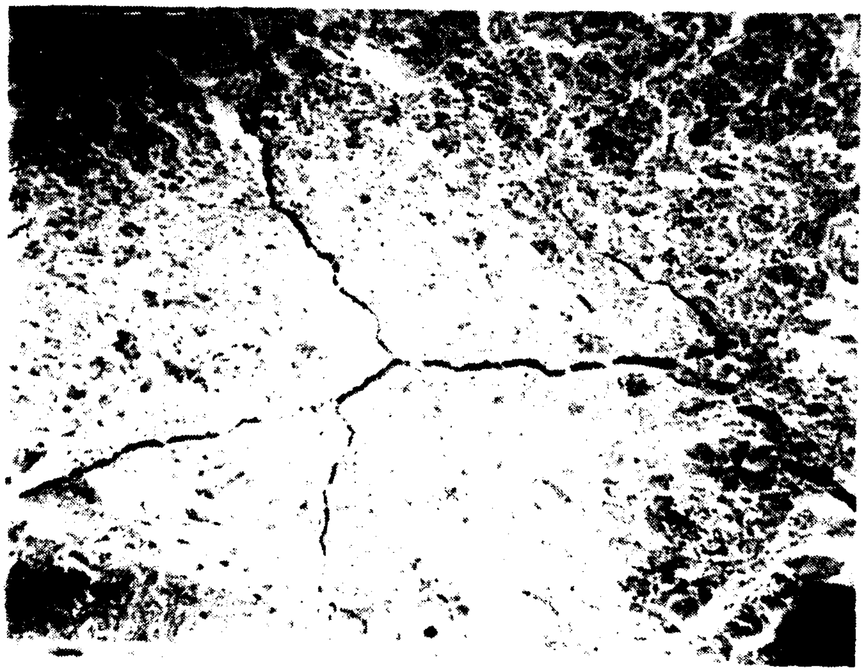

Figure 26. SEM fractograph showing the cracked region outlined on Figure 25, at higher magnification, Mag. 260X.

EXAMINATION OF SURFACE COATINGS

Specimens A and AA were utilized for microscopic examination of the cadmium plating and the paint. Figure 27 is an optical micrograph showing a typical cross-sectional view of the coatings. Regions of the cadmium layer were measured and found to have a thickness range of approximately 0.0003 to 0.0006 inches. These readings conformed to the requirements set forth in MIL-C-8837, Section 3.4.1, which stated that the thickness of the cadmium plating shall be 0.0003 inches, minimum. Figure 28 is a SEM micrograph also containing both coatings. The cadmium plating and the paint layer have been designated on the figure as Area 1 and Area 2, respectively. Further examination of these regions under high magnification revealed no significant signs of faulty adhesion, blistering, peeling, or misplating.

Elemental composition of the coatings was determined by electron dispersing spectroscopy. The resulting spectra obtained from these analyses are shown in Figures 29 and 30. EDS analysis of the paint (refer to Figure 29) revealed a large titanium (Ti) peak. Titanium dioxide is commonly used as a coloring agent in paint pigment. The trace of silicon (Si) detected may have represented extender pigments which are often composed of silicious matter or perhaps remnants of surface greases or lubricating oils that had also been analyzed. Figure 30 contains the spectra of the cadmium plating. The small chromium (Cr) peak, which appeared in both analyses, was indicative of the prior chromate treatment performed on the missile hook as required by MIL-C-8837. The substrate was chromated to retard or prevent formation of white corrosion product on surfaces exposed to certain environments, including marine atmospheres. The small amount of iron (Fe) was associated with the base metal (300M steel).

Specimens B and BB were retained for microscopic examination of the "Microlube" coating. Figure 31 is an optical micrograph of a representative region containing a cross-sectional view of the coating. The chromium-based alloy was identified on the figure as the white layer. This coating was deposited onto the substrate by ion displacement. The dark layer corresponds to the fluorocarbon polymer that was applied by a duplex electroregistration process and used as a friction and corrosion inhibitor. The specimens were etched using Villela's etchant.

Figure 32 is a SEM micrograph showing the chromium and polymer layers. The engineering drawing for the missile hook, (reference Raytheon Drawing No. 685029, Figure 14), stated that the "Microlube" coating shall have a thickness of 0.0008 to 0.0012 inches. The chromium layer had a measured thickness of approximately 0.0004 to 0.0005 inches, while the polymer coating was approximately 0.0008 to 0.0014 inches thick. The total thickness of the "Microlube" coating was 0.0012 to 0.0019 inches, which exceeded the specification. Maximum thickness requirements are prescribed for coatings to insure proper adherence and coherence.

An EDS analysis was conducted of the chromium and polymer layers. Figures 33 and 34 show the resulting spectra obtained from these examinations. The spectra shown in Figure 33 contains those elements associated with the polymer coating. The fluorine (F) peak identifies the base material which is Teflon. Figure 34 contains a large amount of chromium (Cr) which characterizes the chromium plating.

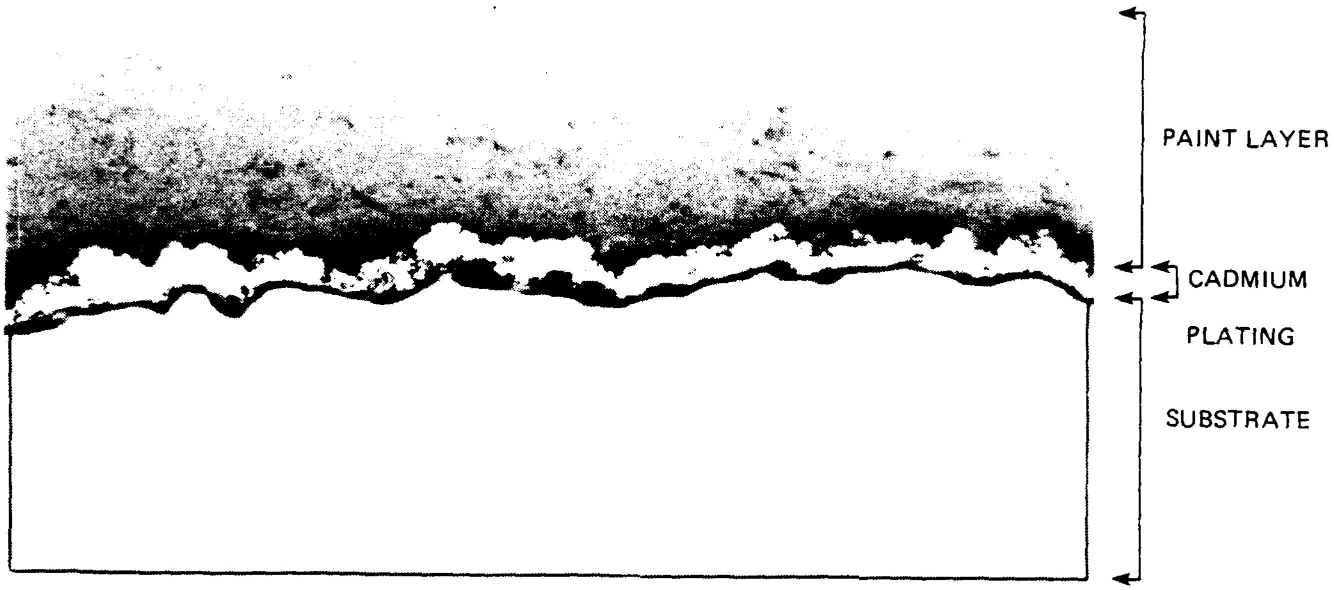

Figure 27. Optical micrograph of the cadmium plating and the paint, Mag. 500X.

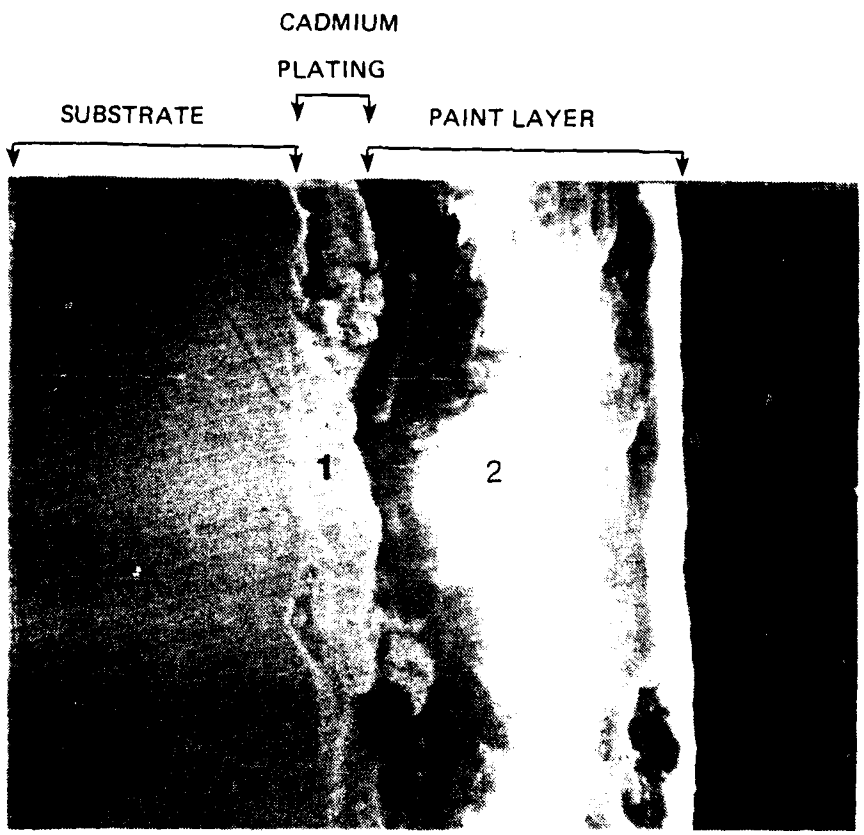

Figure 28. SEM micrograph of the cadmium plating (Area 1) and the paint (Area 2), Mag. 1000X.

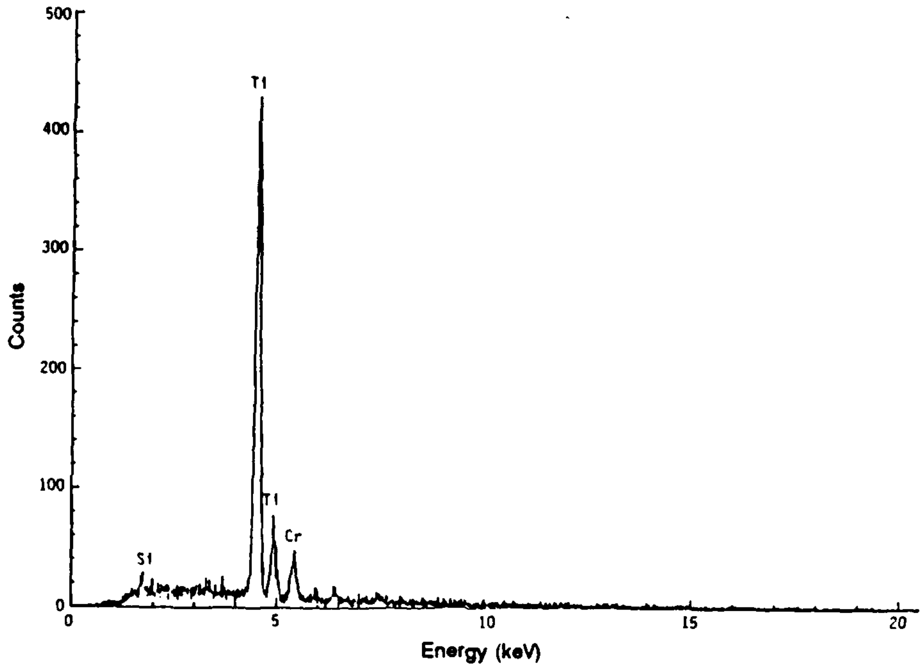

Figure 29. EDS spectra of the paint.

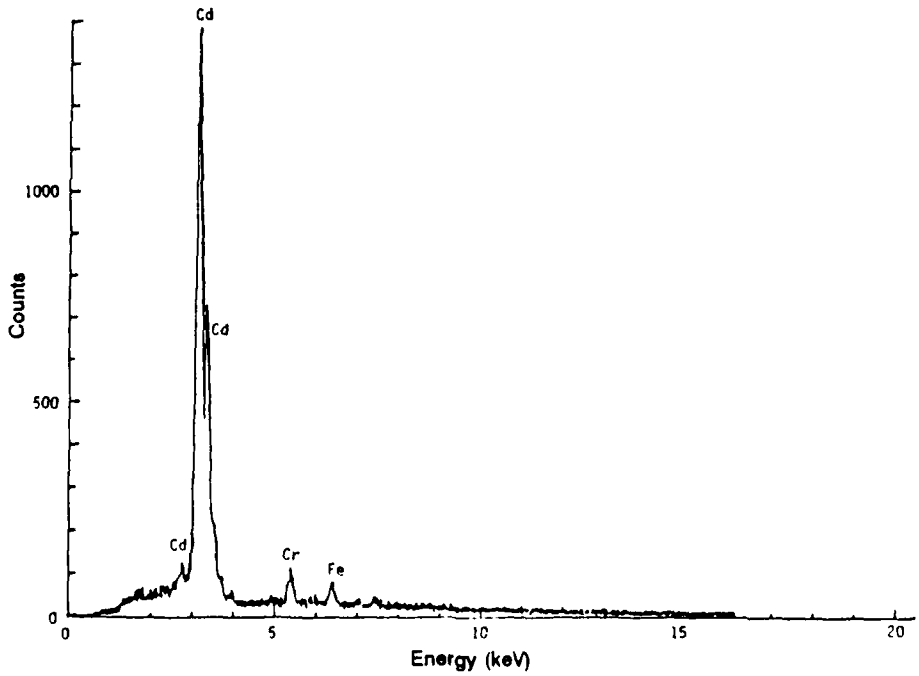

Figure 30. EDS spectra of the cadmium plating.

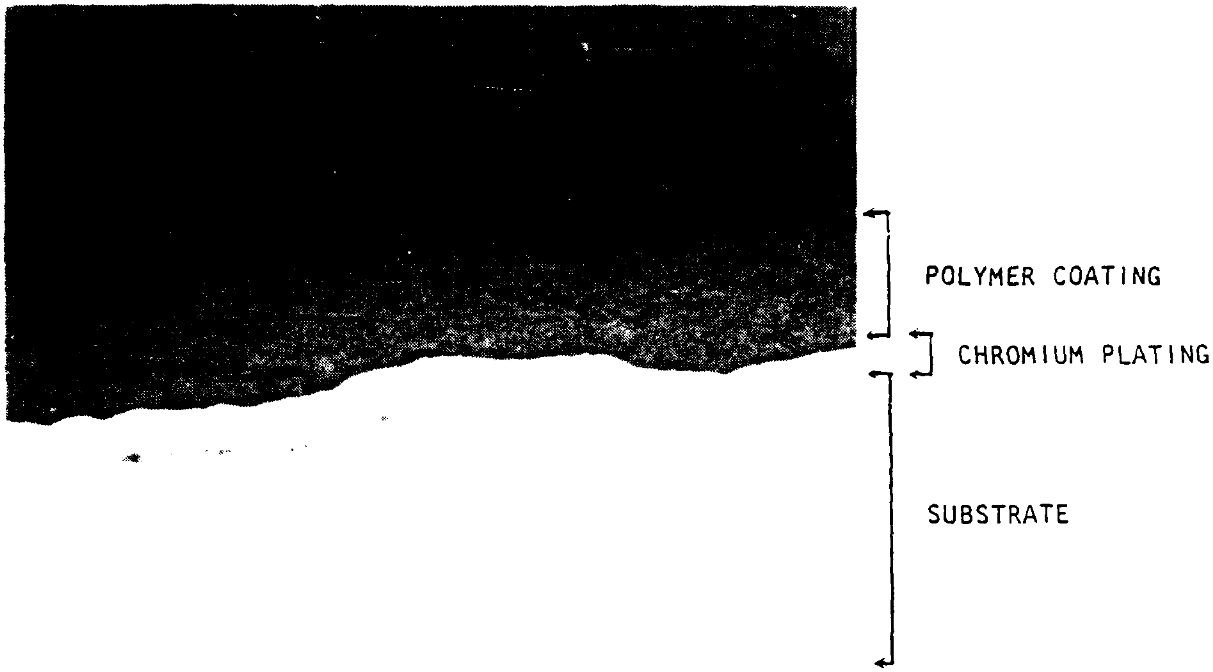

Figure 31. Optical micrograph showing the "Microlube" coating composed of distinct chromium and polymer layers, Mag. 500X.

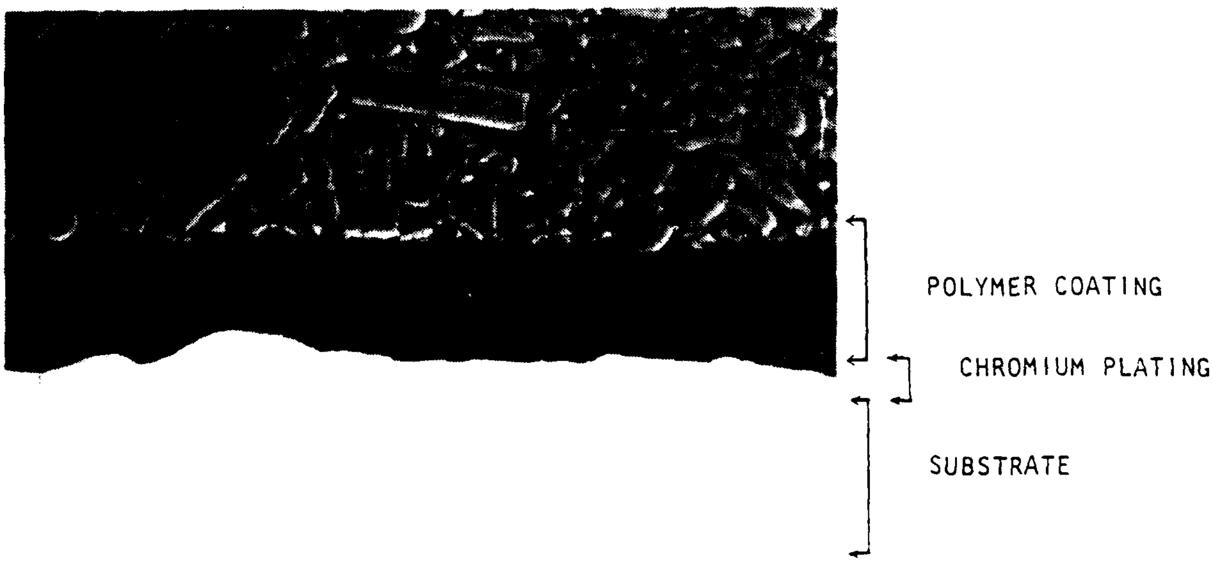

Figure 32. SEM micrograph of the chromium plating and the polymer layer which constitute the "Microlube" coating, Mag. 500X.

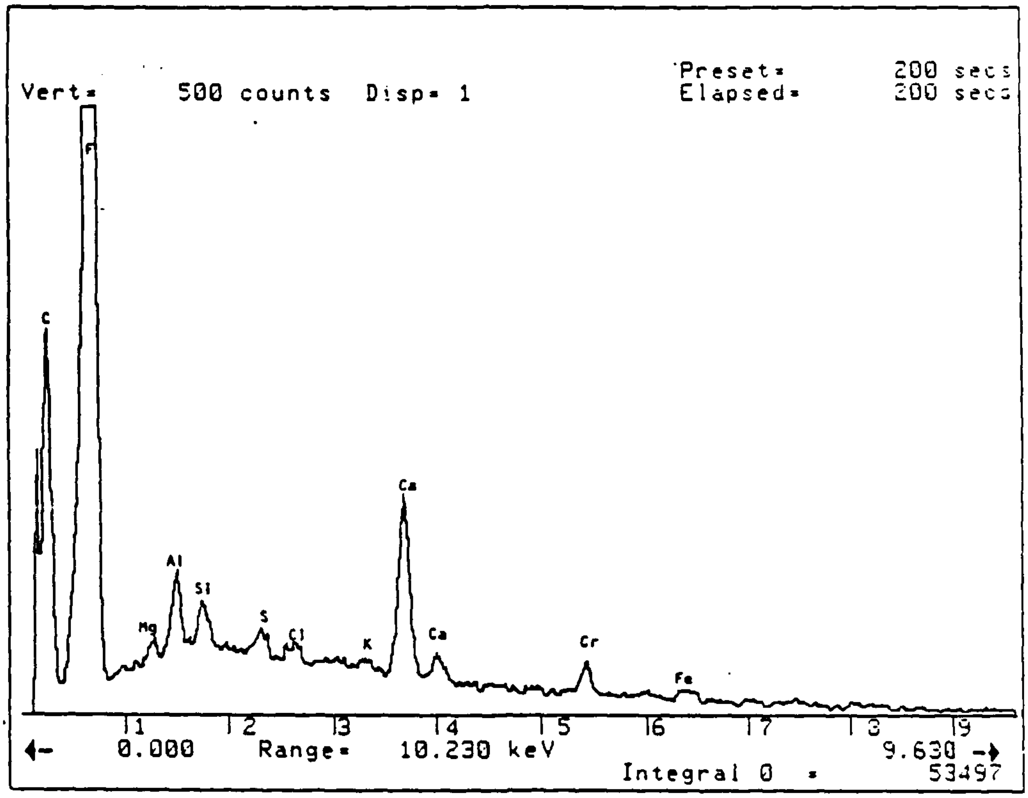

Figure 33. EDS spectra of the polymer coating.

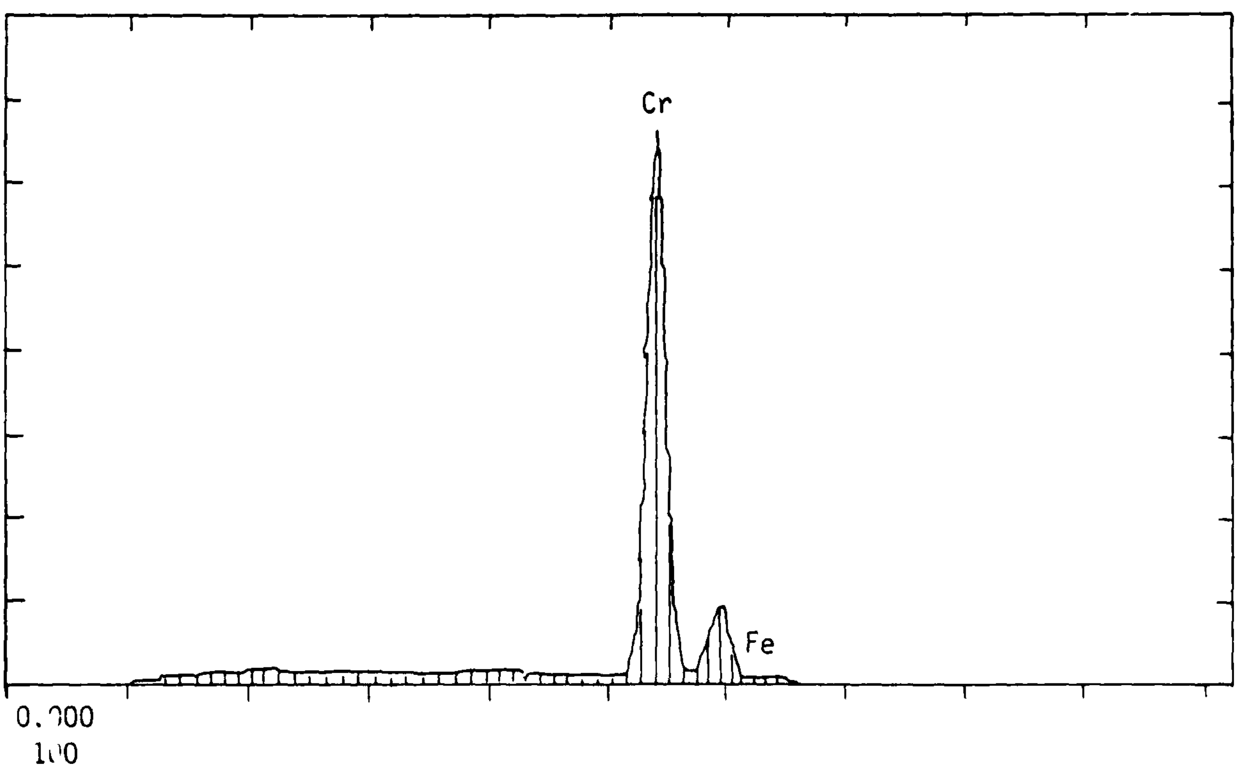

Figure 34. EDS spectra of the chromium plating.

MECHANICS ANALYSIS

A component's ability to sustain tensile loading is adversely affected by a crack. Elevated stress levels along the leading edge of a crack may be sufficient enough to cause sudden rapid crack propagation and, ultimately, catastrophic failure. Even if the stress intensity is not great enough at the crack tip, other factors could significantly contribute to crack growth, such as fatigue. Other influences of crack growth include stress corrosion cracking, hydrogen embrittlement, and corrosion fatigue, which will be discussed later in further detail in regard to the missile hook failure. As the crack area grows, the component's cross-sectional area decreases. Subsequently, the stress intensity near the leading edge of the crack may increase, contributing to greater crack growth. This process continues until the onset of rapid crack propagation and failure. The degree of intensity at the crack tip is a function of the geometry of the part, the type of loading, the length of the crack, and the radius of the crack tip. The intent of this analysis was to determine the following:

1. Calculate the maximum operating stress normal to the fracture face due to the applied loading.

2. Calculate the critical crack size based on published values of fracture toughness for VAR 300M steel.

3. Calculate the critical stress intensity factor (K_{Ic}) for the conditions observed and compare with the published value of fracture toughness for VAR 300M steel.

This information would then be utilized tó evaluate the fracture toughness of the missile hook.

1. The operating loads were determined statically incorporating maximum service loads which included aerodynamic considerations such as "G" force as well as the weight distribution of the Sparrow Missile, as shown in Figure 35.

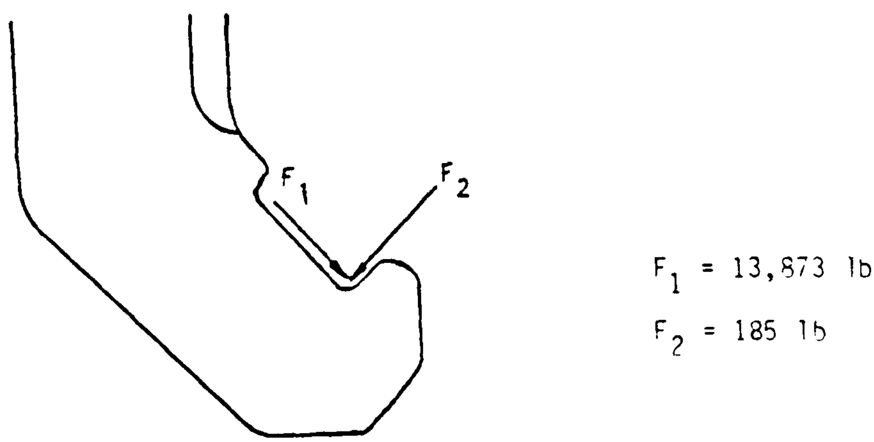

Figure 35. Static loading determined by analysis of maximum service loading, Reference 7. These loads were used to determine the operating stresses at the crack origin.

7. CHERTOCK. *F-14A Sparrow Launcher*. Raytheon Company, Missile Systems Division, Report No. 7150-5B-002, June 1970.

The stresses acting upon a plane normal to the neutral axis of the missile hook were calculated. Pertinent dimensions and locations, such as crack parameters, the neutral axis, cross-sectional areas, and inertias were determined from measurements of the actual component and information obtained from the engineering drawing of the component, "Hook, Locking, Missile" (reference Raytheon Drawing No. 685029, Figure 3).

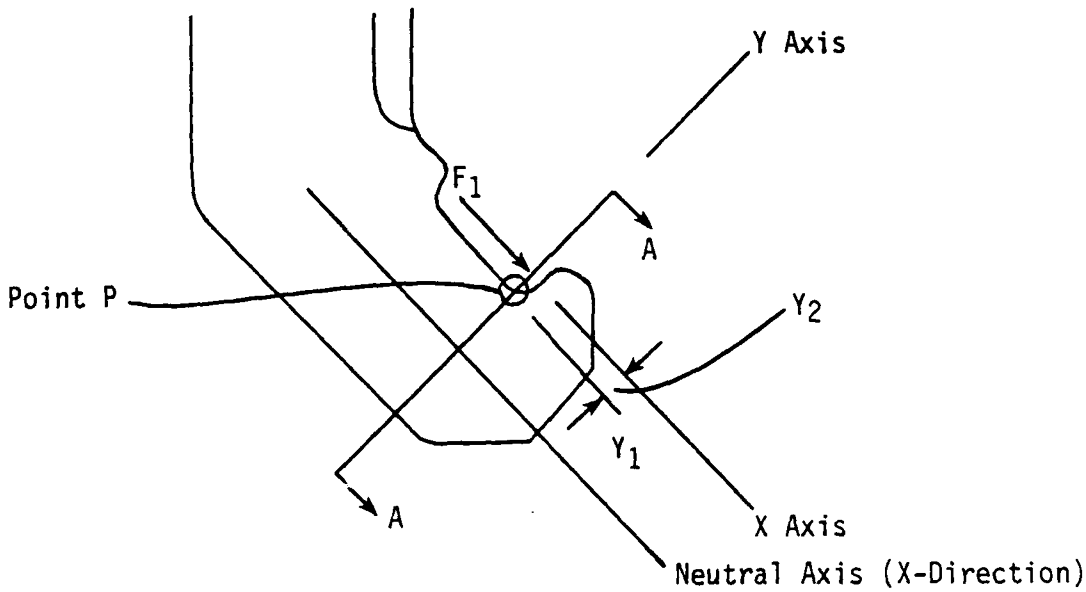

Figure 36. *Face A-A is the surface perpendicular to the neutral axis on which ∇_x and ∇_y were calculated at point P.*

In the X-direction, the stress (∇_x) at the crack site (point P) was the result of the load, F_1 and the moment, M_1. The moment, M_1, was caused by the eccentricity of F_1 a distance Y_1 from the neutral axis (X-direction), as shown in Figure 36, and determined to be (F_1 x Y_1).

$$\nabla_x = F_1/\text{Area}_{A\text{-}A}^{*} + M_1\ (Y_1 - Y_2)/\text{Inertia}_{A\text{-}A}^{*}$$

$$= 13{,}873/0.4742 + 4{,}093.92\ (0.2951 - 0.1045)/0.0062$$

$$= 29{,}255.59 + 125{,}556.69$$

$$= 154.8 \text{ ksi}$$

In the Y-direction, the stress at point P was the result of the load, F_1, and the moment, M_2, acting upon the tip of the missile hook. The moment, M_2, was caused by the eccentricity of F_1 a distance of Y_2 from the crack site, as shown in Figure 37, and determined to be (F_1 x Y_2).

*See Appendix A.

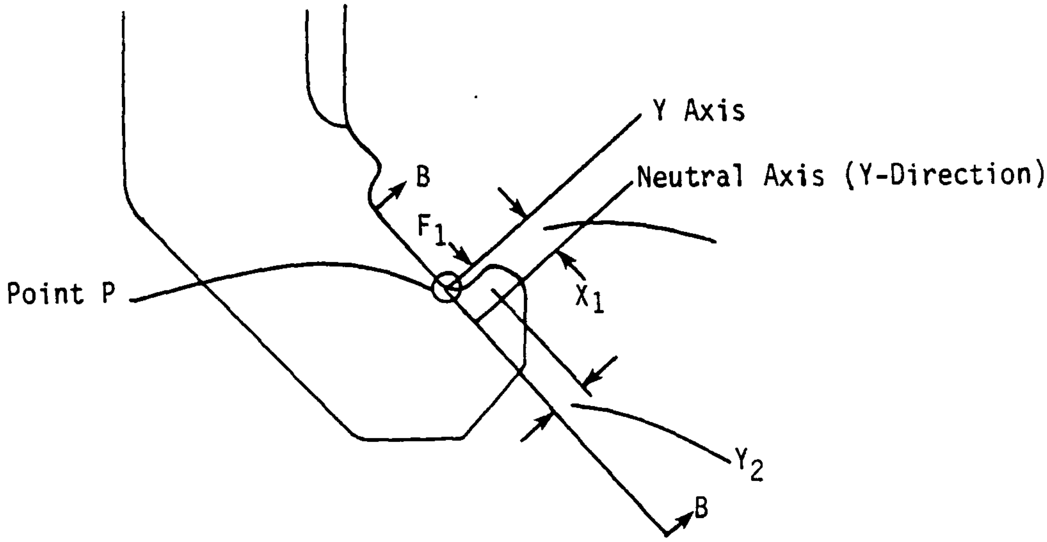

Figure 37. The load F_1 produces a moment about the neutral axis (Y-direction) which induces a stress σ_y at point P.

$\nabla_y = M_2X/\text{Inertia}_{B\text{-}B}$*

$= 1469.27\ (0.1045)/(0.00361)$

$= 42.54$ ksi

While the load F_2 produces a shear stress across Face A-A, the shear stress (σ_{xy}) at point P is zero as the distribution of shear across the face is a paraboia with a maximum value at the centroid.

*See Appendix A.

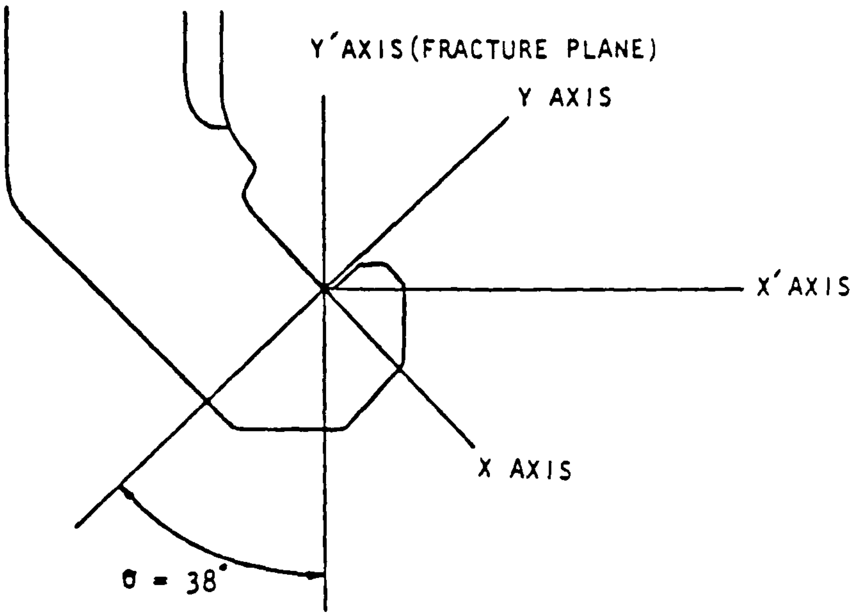

Figure 38. The angle between the fracture plane and the plane about which stresses were calculated.

Since the fracture plane did not coincide with Section A-A, see Figure 38, the stress across the fracture place must have been greater than that across Section A-A. From this conclusion, the stress across the fracture plane can be approximated, $\nabla_{x'} \geq \nabla_{x}$. Therefore, $\nabla_{x'}$ = 154.8 ksi was used to calculate the critical crack stress intensity factor.

2. It was possible to measure the critical crack size from the failed component. This area had been previously identified as Zone 1 (see Figure 2) or the "thumbnail" crack region. The crack parameters and pertinent dimensions of the missile hook were obtained from measurements of the fracture surfaces, as shown in Figure 39.

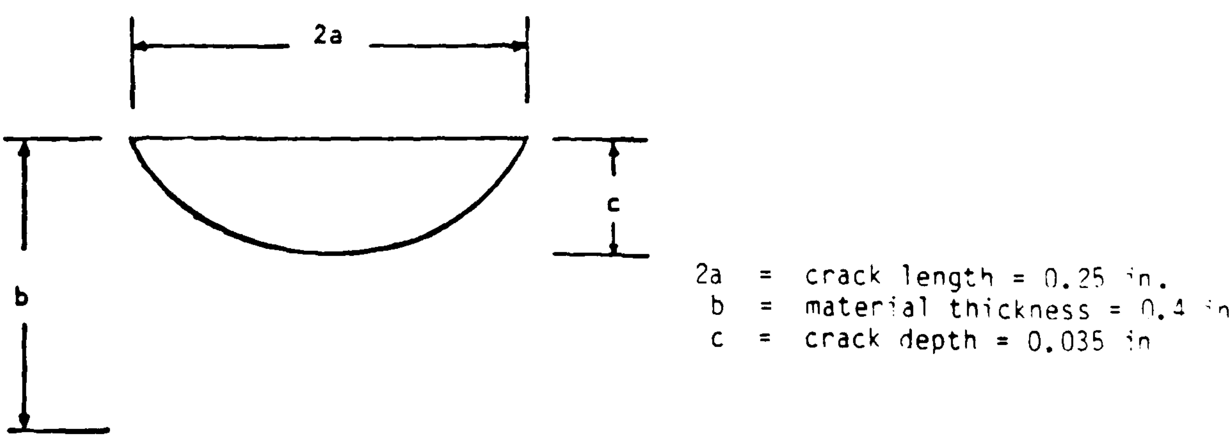

Figure 39. Crack parameters measured from the fracture surface.

Based upon the type of loading, and the geometry of the crack and the missile hook, a model of a semielliptical crack in a slab subjected to a uniform uniaxial tensile stress was selected to determine the critical crack depth at which failure would occur. While this model is a simplification of the actual geometrical configuration of the crack and missile hook, the results obtained can be utilized to evaluate the relative toughness of the material. Since the crack depth, c, is very shallow compared to the length of the fracture (2a), only the axial K_I stress intensity case was considered, as shown in Figure 40.

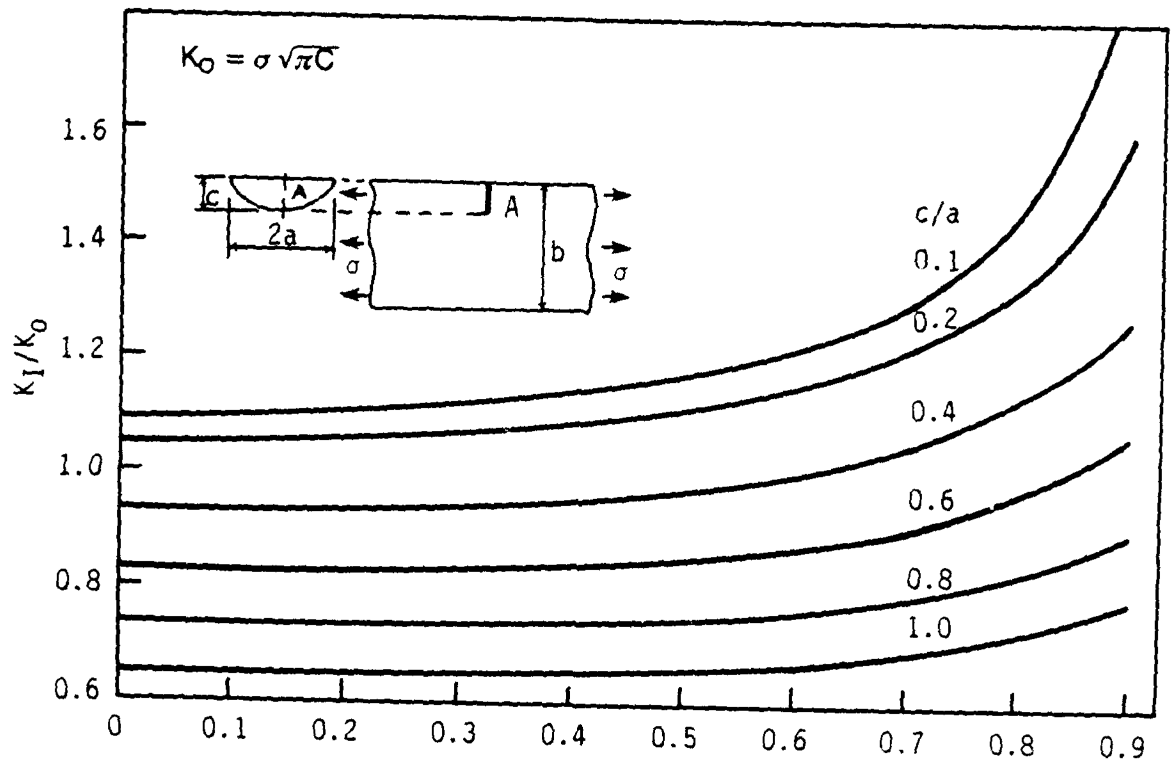

Figure 40. Graph relating stress intensity factor to crack parameter ratios, Reference 8.

A stress intensity factor K_I/K_o was determined graphically (Figure 40) from an established plot of values. This factor is based upon certain ratios of crack parameters.

Since c/a = 0.28 and c/b = 0.0875, the stress intensity ratio was determined to be K_I/K_o = 0.99.

The normalized stress intensity equation for uniaxial tensile loading of an infinite bar containing a semielliptical crack; $K_{oT} = \sigma x' \sqrt{\pi C}$[8] was utilized to calculate the theoretical critical crack depth (C) since K_{oT} can be expressed as $K_{IC}/(K_I/K_o)$[8] and a published value of K_{IC} was incorporated.

Where:

K_{oT} = normalized stress intensity factor,

$\sigma x'$ = stress normal to the fracture face; 154.8 ksi,

C = crack depth; 0.035 in.,

K_{IC} = critical stress intensity factor (published value, 55.9 ksi),[9] and

K_I/K_o = stress intensity ratio (refer to Figure 40, 0.99).

Therefore, by substitution:

$$C = \{K_{IC}/[\sigma x'(K_I/K_o)]\}^2/\pi$$

$$= \{55.9/[154.8(0.99)]\}^2/\pi,$$

theoretical critical crack depth = 0.0424 in., and

actual crack depth = 0.035 in.

3. Utilizing the operating stresses calculated in Section 1 and the critical crack dimensions measured from the failed component, the critical stress intensity factor, K_{IC}, was determined based on the observed conditions.

$$K_{IC} = (\sigma x' \sqrt{\pi C})\ (K_I/K_o)$$

Where:

K_{IC} = critical stress intensity factor for the crack geometry observed:

$$K_{IC} = 154.8 \sqrt{\pi (0.035)} \quad (0.99)$$

$$= 51.3\ (0.99)$$

$$= 50.8 \text{ ksi } \sqrt{\text{in.}}$$

For purposes of comparison and evaluation, published values of the plane-strain fracture toughness for VAR 300M steel having approximately the same tensile strength as the failed component were included. These values ranged from 55.9 ksi $\sqrt{\text{in.}}$ in the transverse WW orientation to 52.2 ksi $\sqrt{\text{in.}}$ in the longitudinal direction.[9]

8. ROOKE, D. P., and CARTWRIGHT, D. J. *Compendium of Stress Intensity Factors*. Her Majesty's Stationary Office, London, 1976, p. 297-299.

9. *Ultra-High Strength Steel*. ASM Metals Handbook, Properties and Selection Iron and Steel, v. 1, 9th ed., 1978, p. 429

The threshold stress intensity for stress corrosion cracking (K_{Iscc}) is approximately 14.5 ksi $\sqrt{in.}$[10] for the steel under investigation. This value was included within the context of this analysis since the missile hook had been exposed to a salt water environment. The influence of corrosion can be a significant factor when determining the useful service life of a component.

In summary, since the calculated critical size (0.42") was greater than actual measurements of crack depth (0.35"), the material did not appear to exhibit the anticipated fracture toughness. The size of the crack that caused the failure should have been larger. Similarly, the value of K_{Ic} (50.8 ksi) calculated for the observed conditions was lower than published values, which also supports this conclusion.

10. *Ultra-High Strength Steel.* ASM Metals Handbook, Properties and Selection Iron and Steel, v. 1, 9th ed., 1978, p. 428.

DISCUSSION

Fatigue Failures

Failures resulting from fatigue generally consist of three stages: crack initiation, crack propagation until criticality is attained causing catastrophic failure, and final fast fracture. Fatigue cracks initiate in regions where the stress is most severe. In this investigation, the undercut radius of the missile hook acted as a stress concentration area where a crack originated. The most characteristic macroscopic features associated with fatigue crack propagation are beach marks. Figure 15 reveals evidence of beach marks that formed during periods of crack arrest. Another prominent feature found on fatigue-fracture surfaces during electron microscopy are fatigue striations. Figure 18 contains these finely spaced markings which were the result of a single cycle of stress. The clarity of the striations observed on the fracture surface of the missile hook was adversely affected by corrosion. The final fast fracture zone of a material, such as VAR 300M steel, normally consists of two modes; the first being a tensile fracture (plane-strain mode) which extends from the fatigue region in the same place. Within the tensile fracture, radial marks, or chevron patterns, form. Figure 15 contains radial marks which point back to the crack origin, located in Zone 1 of the missile hook fracture. Zone 2 and Zone 3 represent the tensile fracture which proceeds from Zone 1, the fatigue region. The second fracture mode would be shear fracture (plane-stress mode) at 45° to the surface of the component bordering the tensile fracture. This mode of failure, also referred to as shear lips, was identified on the fracture surface of the missile hook, as shown in Figure 22. The evidence collected during the failure analysis of the missile hook strongly indicates that the failure was the result of a fatigue crack that had initiated at the base of an undercut radius on the machined lip of the component. As the crack propagated from the fatigue zone (Zone 1) the cross section of the component slowly decreased and final fast fracture occurred. The duplication of the original failure by laboratory tests of a similar component would be required to establish and confirm the precise mode of failure. Such testing should determine if corrosion fatigue was the primary mechanism of failure.

Stress Corrosion Cracking and Hydrogen Embrittlement

High strength steels can fracture under very low static stresses when exposed to an environment capable of causing stress corrosion cracking (SCC) or if they have been embrittled as a result of hydrogen absorption. Energy dispersive spectroscopy was used to analyze the fracture surface and deposits of Zone 1 on the missile hook. There were no traces of any contaminants found that would render the alloy particularly susceptible to SCC. Hydrogen embrittlement (HE) fractures occur when a sufficient amount of atomic hydrogen permeates into the metal and causes cracking. As the strength level of the steel and the hydrogen concentration increases, the tendency for embrittlement would also increase. Hydrogen may also induce SCC and usually produces sharp singular cracks in contrast to the extensive branching normally observed in typical SCC failures. Stress corrosion and HE fractures in high strength steels occur primarily by intergranular decohesion, or in a trangranular fashion, and do not contain fatigue beach marks.. Fractographic examination did not support the conclusion that the missile hook failure was primarily caused by SCC or HE.

Corrosion Fatigue

Failures resulting from corrosion fatigue (CF) are caused by a reduction of fatigue resistance due to the presence of a corrosive environment. Some of the governing variables that influence CF in high strength steels include: the load frequency, the stress ratio, the

environment, and the stress intensity range. Most CF cracks originate at small flaws or at local stress raisers and propagate as a crystallographic crack, producing cleavage type or intergranular fractures. These modes of failure were not observed on the fracture surface of the missile hook. As the CF crack proceeds across the component, it changes to a non-crystallographic crack. The microfractographic features of CF may be the same as those of typical fatigue failures except that they may be obscured by corrosion products. Fractographic examination of the missile hook showed that much of Zone 1, indeed, exhibited extensive corrosion, making it difficult to conclude the mechanism of crack initiation in this region.

Fatigue, as well as CF cracks, may initiate from pits or cracks caused by other mechanisms of failure, such as SCC. Secondary cracks were observed originating from corrosion pits on surfaces adjacent to the primary fracture, as shown in Figure 24. Both SCC and CF can take place when the maximum stress intensity factor (K_I) exceeds the K_{ISCC}. The calculated K_{IC} value of the component was much greater than the K_{ISCC}. Therefore, when exposed to certain environmental conditions, the material would be susceptible to these mechanisms of failure.

The theoretical critical crack depth was determined to be 0.0424 inches, while the measured value was approximately 0.035 inches. The calculated K_{IC} for the conditions observed was approximately 50.8 ksi $\sqrt{in.}$, while published values for VAR 300M steel ranged from 52.2 ksi $\sqrt{in.}$ to 55.9 ksi $\sqrt{in.}$. The differences between the theoretical figures and those based on test data indicate that the material used to fabricate the missile hook exhibited a lower fracture toughness than anticipated, assuming that the mathematical models used in the fracture mechanics analysis were accurate. Since the material did not display any unusual microstructural characteristics and satisfied specified strength requirements, it was concluded that the primary cause for a reduction in fracture toughness would be attributable to the effects of corrosion.

The values obtained as part of the fracture mechanics analysis are approximations that have been incorporated into the Conclusions of this report as such. It is important to note that any or all of the mechanisms of failure previously discussed may be operative as crack growth occurs. In summary, the missile hook failure displayed characteristics often associated with CF, however, based upon the analysis of the fracture mode observed in Zone 1, it could not be concluded that CF was the dominating mechanism of failure.

CONCLUSIONS

1. The radius along the machined lip of the missile hook was undercut and measurements of the upper radius found it to be sharper than specifications allowed. It was determined that a fatigue crack had initiated at the base of the undercut radius which had acted as a localized stress raiser.

2. Chemical analysis verified that the missile hook was fabricated from VAR 300M steel. The microstructure was tempered martensite, indicative of the heat treating process utilized. There were no signs of grain refinement or any areas found that contained unusual precipitation or coagulation of carbides, which may have been present if the material had been locally heated as a result of excessive grinding or rubbing. There were also no large inclusions present. In this condition, the alloy should have had a good combination of strength, toughness, and fatigue resistance.

3. Visual inspection and light optical microscopy revealed evidence of extensive surface pitting on load-bearing regions adjacent to the fracture. In these locations, the "Microlube" coating had been completely worn away during service. Corrosion pits had also served as localized stress concentration areas and had initiated cracks in some instances.

4. Hardness measurements taken of transverse and longitudinal sections of the missile hook, when converted to tensile strength values, confirmed that the strength of the material satisfied requirements.

5. The polymer layer, which is a component of the "Microlube" coating system, exceeded maximum thickness requirements. Thickness parameters are defined to maximize the service life of the coating by insuring proper adherence and coherence. The remaining coatings inspected met required thickness ranges and uniformity specifications. There were no signs of faulty adhesion or misplating of areas examined where the coatings were still intact. However, the "Microlube" coating that was placed over the surface of the load-bearing region was severely damaged by excessive wear and, consequently, corrosion pitting was allowed to take place.

6. Light and scanning election microscopy of the fracture surfaces showed topographies consistent with the characteristics of a fatigue crack. The progression marks and fatigue striations found were indicative of an advancing crack front that slowly propagated until the stress parameters of the material were exceeded and fast fracture occurred. The dark corrosion layer covering the fatigue crack region remained as evidence verifying that this area was the result of a preexisting crack that had been exposed to a marine environment for a longer period of time than the region of fast fracture which contained very little corrosion. Microscopic examination did not reveal that crack initiation was attributed to a corrosion pit, a surface discontinuity, or an inherent material defect.

7. The fracture mechanics analysis yielded a K_{Ic} value for the conditions observed that was lower than published values of K_{Ic} for VAR 300M steel. The calculated critical crack size was larger than the actual crack size of the failed component. This information suggests that the fracture toughness of the material was slightly lower than expected. This was attributed to the effects of corrosion, since published values of K_{Iscc} were as low as 14.5 ksi $\sqrt{\text{in.}}$.

8. The evidence collected in conjunction with the failure analysis investigation of the missile hook favors a failure mode attributable to a fatigue crack that had initiated at the base of the undercut radius on the machined lip of the missile hook.

RECOMMENDATIONS

1. Insure that the radius on the machined lip of the missile hook is manufactured according to specification.

2. Finite element analysis and/or flight simulated tests should be conducted on the missile hook to determine the maximum operating stresses at critical points. This information could then be utilized to investigate the possibility of replacing the VAR 300M steel used to fabricate the component with a tougher and more corrosion resistant material.

3. An inspection of missile hooks currently in service should be conducted to detect cracks, corrosion pitting, and exposed steel surfaces according to the procedure outlined below:

Inspection Procedures

(a) Visual examination and the liquid penetrant test, performed in accordance with MIL-STD-6866, should be utilized to reveal evidence of cracks open to the surface. Parts that contain such defects should be removed from service and discarded.

(b) Inspection for corrosion pitting can be performed visually with the aid of a magnifying lens. Components showing any degree of pitting should be replaced immediately.

(c) Exposed steel surfaces can easily be distinguished by the methods outlined in sections (a) and (b). The machined lip of the missile hook which is an area subjected to friction during loading and exposed to a marine environment needs to be properly cleaned and recoated.

4. It is suggested that a dry film lubricant conforming to MIL-L-23398D (Lubricant, Solid Film, Air-Cured, Corrosion Inhibiting) be used to replace the damaged and worn "Microlube" coating on fielded components. The dry film lubricant should conform to the following requirements:

Film Lubricant Characteristics and Requirements

(a) To insure compatibility, the solid dry film lubricant should contain polytetrafluoroethylene (PTFE) as the lubricating solid since the polymer layer of the "Microlube" coating consists of a Teflon-based material.

(b) The lubricant should not contain graphite because, in the presence of an electrolyte such as salt water, accelerated corrosion of the electropositive component (the steel missile hook) can occur.

(c) The recommended cured film thickness is from 0.0002 to 0.0005 inches which is best attained incorporating an air cured, aerosol propelled (Type II), solid dry film lubricant.

(d) Optimum performance of a dry film lubricant requires that adequate surface preparation be performed on areas to be coated. When properly applied and cured, the lubricant will decrease the coefficient of friction and reduce wear between the mating components in motion while providing a protective barrier against corrosion. The lubricant will also resist adhesion of lint, dust, and other kinds of fallout encountered in service.

5. The proceeding section discusses recommended procedures for cleaning the machined lip of the component. These instructions have been formulated taking into consideration that all of the required work associated with cleaning and applying the lubricant must be accomplished out in the field, and also while the part is still attached to the aircraft.

Surface Preparation

(a) It is strongly advised that all surface contaminants be removed such as greases, oils, dirt, water, oxides, and also the loose, blistered remains of the "Microlube" coating. This can be accomplished by the combination of suitable solvent and detergent cleaners along with a prescribed mechanical surface conditioning method.

(b) According to Claus,[11] a 3-dimensional nonwoven abrasive product can be used effectively to remove general corrosion and deteriorated coatings mechanically while generating a surface profile which serves as an exceptional base for the dry film lubricant. These products are composed of a fiber, resin, and mineral. When used properly, they provide a controlled cutting action that facilitates removal of surface materials without dangerously undercutting or gouging. A wide variety of aggressiveness can be selected ranging from one form that will not even scratch glass to another which will abrade hardened steel.

6. During the regular monthly inspection and maintenance procedures performed on the aircraft, it is recommended that the dry film lubricant coating and adjacent areas on all missile hooks be inspected under the criteria discussed previously.

ACKNOWLEDGMENT

The request for this failure analysis was initiated by Mr. Stephen Keller of the Pacific Missile Test Center.

The authors wish to extend thanks to Mr. Francis Baratta, Dr. Sharad Pednekar, and Mr. Andrew Zani for their helpful discussions.

11. CLAUS, J. J. *Surface Conditioning Products as Tools for Corrosion Removal and Corrosion Prevention.* Proceedings of the 1987 Tri-Service Conference on Corrosion, AFWAL-87-4139, v. 11, p. 205-219.

APPENDIX A.

Determination of Cross Section A-A Area

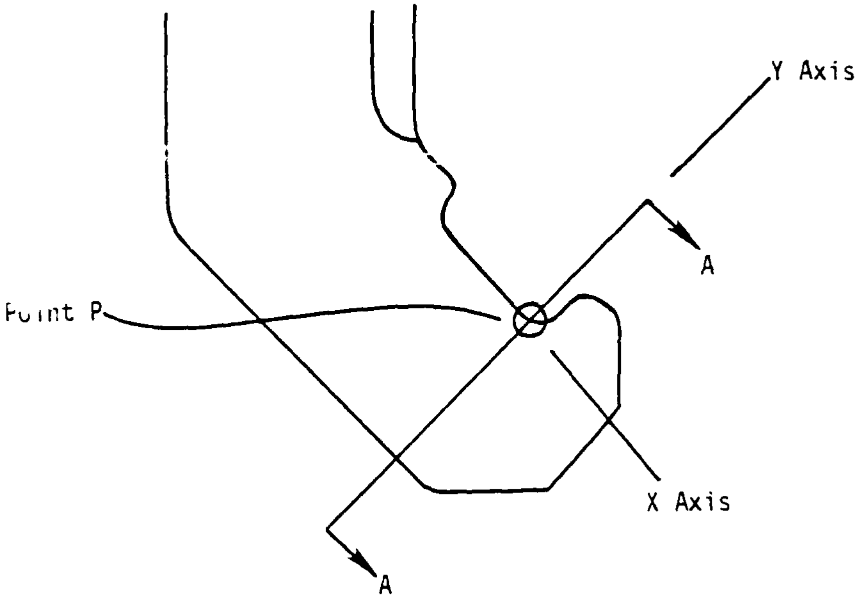

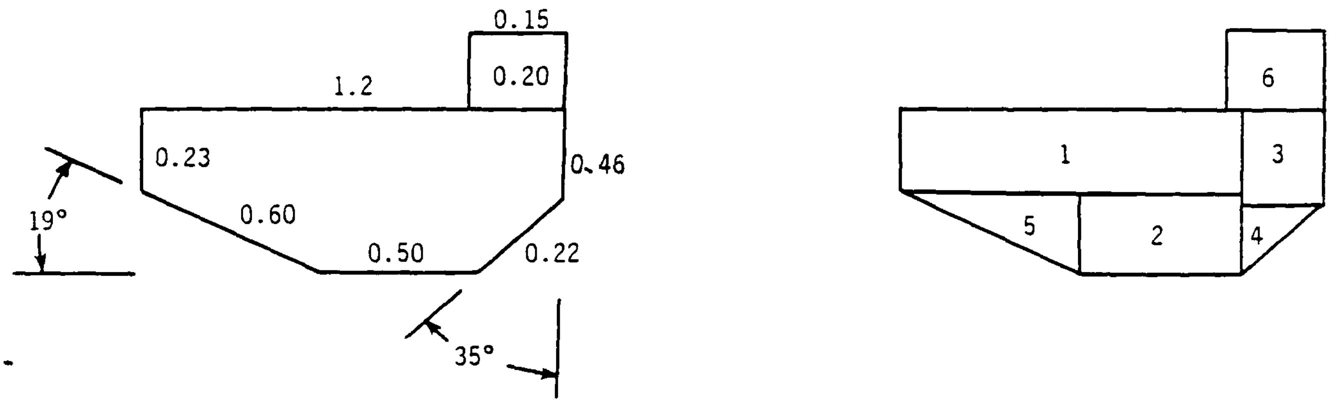

View A-A

Section No.		Area (in.^{2})
1	$0.23\,(1.2 - \sin 35°\,(0.22))$	= 0.24697
2	$0.5\,(0.6 \sin 19°)$	= 0.09767
3	$0.26\,(\sin 35°\,(0.22))$	= 0.03281
4	$(0.22)^2 \sin 35° \cos 35°\,(0.5)$	= 0.011358
5	$(0.60)^2 \sin 19° \cos 19°\,(0.5)$	= 0.055397
6	$0.20\,(0.15)$	= 0.03

Total Area = 0.474 in.^{2}

Determination of Neutral Axis Through Section A-A

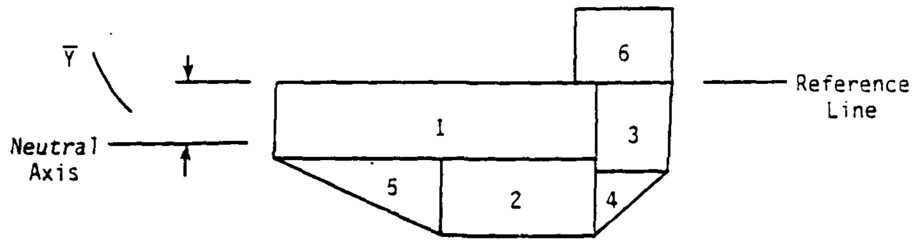

$\overline{Y}$ is the distance from the neutral axis to a reference line. $\overline{Y}$ can be calculated for simple figures such as rectangles, triangles, and circles. By taking the complex cross-sectional geometry of face A-A and dividing it into sections of rectangles and triangles, $\overline{Y}$ can be found by the formula:

$$\overline{Y} = \Sigma A_i\bar{y}_i / \Sigma A_i$$

where $\Sigma A_i y_i$ is the sum of the first moment of areas of each section.

ΣA_i is the sum of the areas of each section.

$\bar{y}_i$ is the distance from the reference line to the centroid of each section:

Calculating $\bar{y}_i$ for each section:

Section No.		$\bar{y}_i$ (in.)
1	0.5 (0.23)	= 0.115
2	0.23 + 0.5 (0.6 sin 19°)	= 0.32767
3	0.5 (0.26)	= 0.13
4	0.26 + cos 35° (0.22)/3	= 0.32007
5	0.23 + (0.60) sin 19°/3	= 0.295113
6	0.5 (0.2)	= 0.10

Calculating the first moment of area $A_i y_i$ for each section.

Section No.	Area	y_i	$A_i\bar{y}_i$ (in.^{3})
1	0.24697	(0.115)	= 0.02840155
2	0.09767	(0.32767)	= 0.0320035
3	0.0328086	(0.13)	= 0.00426512
4	0.011358	(0.32007)	= 0.00363537
5	0.055397	(0.295113)	= 0.01634837
6	0.03	(0.10)	= 0.003

Summing the first moment of areas:

$$\Sigma A_i y_i = 0.0876539 \text{ in.}^3$$

$\bar{Y} = \sum A_i y_i / A_{total}$

$= 0.0876539/0.4742$

$= 0.184845845$ inch.

Determination of inertia about reference line for each section

Inertia of a rectangle about its centroid	$= 1/12\ bh^3$ (Ref. 12)
Inertia of a rectangle about its base	$= 1/3\ bh^3$ (Ref. 12)
Inertia of a triangle about its centroid	$= 1/36\ bh^3$ (Ref. 12)
Inertia of a triangle about its base	$= 1/12\ bh^3$ (Ref. 12)

where b = base length
h = height length.

To determine the inertia of a figure about an axis parallel to an axis through its centroid requires the parallel - axis theorem:

$$I = \bar{I} + Ad^2 \text{ (Ref. 12)}$$

where I = inertia about an axis parallel to an axis through centroid

$\bar{I}$ = inertia about an axis through centroid

A = area of figure

d = distance from one axis to the other.

The inertia of surface A-A about an axis through point P may be obtained by summing the inertia of each section about the same axis (Ref. 13).

Section No.		I_i (in.^{4})
1	$(0.23)^3\ (1.2 - \sin 35°\ 0.22)/3$	= 0.004355028
2	$0.5\ (0.6 \sin 19°)^3/12 + 0.09767\ (0.32767)^2$	= 0.010796977
3	$(0.26)^3\ (\sin 35°\ 0.22)/3$	= 0.0007392865
4	$(0.22 \sin 35°)\ (0.22 \cos 35°)/36 + 0.011358\ (0.22 \cos 35°/3 + 0.26)^2$	= 0.00118402
5	$(0.60 \cos 19°)\ (0.60 \sin 19°)^3/36 + 0.055397\ (0.60 \sin 19°/3 + 0.23)^2$	= 0.004942004
6	$(0.20)^3\ (0.15)/3$	= 0.0004

12. BEER, F. P., and JOHNSTON, E. R., Jr. *Mechanics of Materials.* McGraw-Hill, New York, 1981, p. 582.
13. BEER, F. P., and JOHNSTON, E. R., Jr. *Mechanics of Materials.* McGraw-Hill, New York, 1981, p. 582.

Summing the inertia:

$$\Sigma I_i = 0.022417315$$

This is equivalent to the inertia of surface A-A. To obtain the inertia of the surface about its neutral axis requires the parallel axis theorem:

$$I = \bar{I} + Ad^2$$

With the calculated inertia of face A-A about an axis through point P, the inertia through the centroid can be determined:

$$\bar{I} = I - Ad^2$$
$$= 0.022417315 - (0.4742036)\ (0.184845845)^2$$
$$= 0.006214732 \text{ in.}^4$$

Determination of cross section B-B inertia.

First, the area of cross section B-B must be calculated.

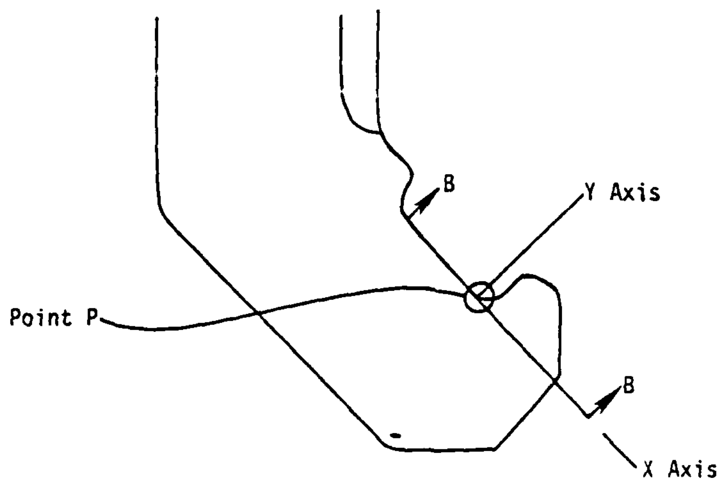

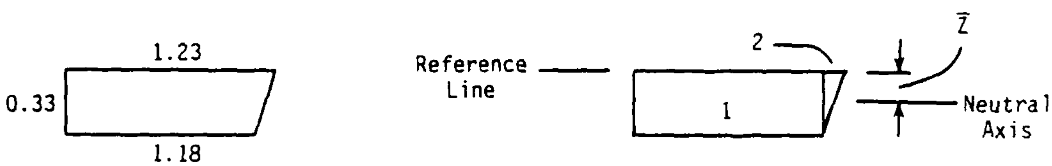

View B-B

Section No.		Area (in.^{2})
1	1.18 (0.33)	= 0.3894
2	0.05 (0.33)/2	= 0.00825

Total Area = 0.39765 in.^{2}

The first moment of areas for each section is found and totaled.

Section No.		$A_i z_i$ (in.^{3})
1	1.18 (0.33) (0.165)	= 0.064251
2	[0.05 (0.33)/2] (0.33/3)	= 0.0009075

Summing the first moments:

$\Sigma\, A_i z_i = 0.0651585$ in.^{3}

The neutral axis in the z direction (perpendicular to the X-Y plane) is then found by the equation:

$$\bar{Z} = \Sigma\, A_i z_i / \Sigma\, A_i$$
$$= 0.0651585/0.39765$$
$$= 0.163858921 \text{ in.}$$

The inertia of the entire cross section of the component is the sum of the inertias of each section. The inertia about the reference line for each section is calculated below.

Section No.		I_i (in.^{4})
1	$1.18\ (0.33)^3/3$	= 0.01413522
2	$0.05\ (0.33)^3/12$	= 0.000149737

Summing the inertia:

$\Sigma\, I_i = 0.014284957$ in.^{4}

To determine the inertia about the neutral axis of surface B-B, the parallel axis theorem is used:

$$\bar{I} = I - Ad^2$$
$$= 0.014284957 - (0.39765)\ (0.163858921)^2$$
$$= 0.00361 \text{ in.}^4$$

With respect to the missile hook tip (the portion of the missile hook above surface B-B), the location of the neutral axes in the X and Y directions was calculated using procedures illustrated previously.

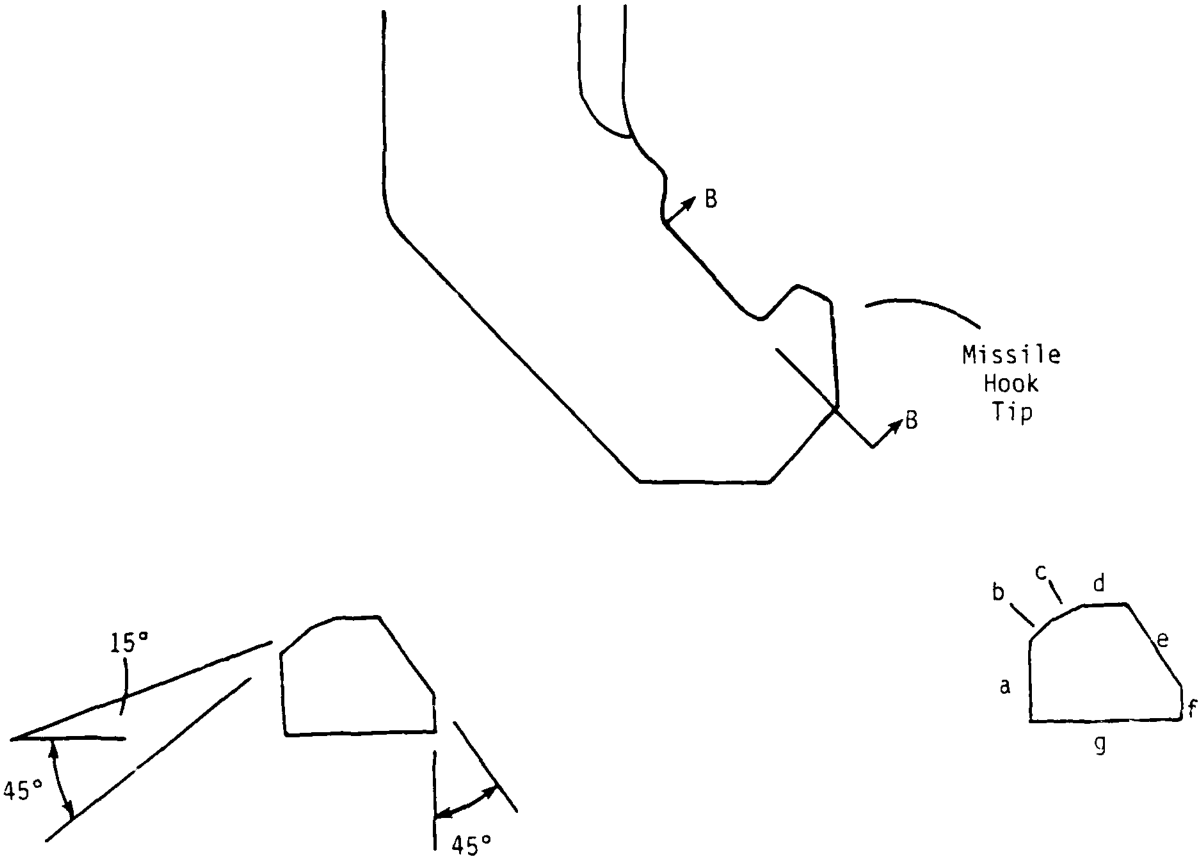

Missile Hook Tip Geometry

<u>Dimensions (in.)</u>

a = 0.20	e = 0.25
b = 0.05	f = 0.07
c = 0.04	g = 0.33
d = 0.08	

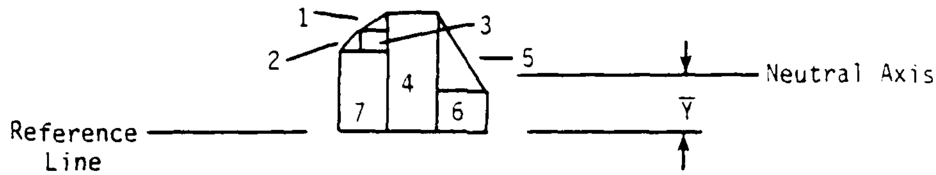

Area of Sections

Section No.		Area (in.^{2})
1	0.04 cos 15° (0.04 sin 15°) 0.5	= 0.0002
2	$(0.05 \cos 45°)^2$ (0.5)	= 0.000625
3	(0.05) cos 45° (0.04) cos 15°	= 0.001366
4	0.24 (0.08)	= 0.0192
5	$(0.25)^2$ sin 45° cos 45° (0.5)	= 0.015625
6	0.07 (0.25) cos 45°	= 0.012374
7	0.20 (0.05 cos 45° + 0.04 cos 15°)	= 0.014798

Calculating $\overline{Y}$, the distance to the neutral axis in the y direction from the reference line:

Distance to reference line for each section:

Section No.		$\bar{y}_i$ (in.)
1	0.04 sin 15° (1/3) + 0.05 cos 45° + 0.20	= 0.2388
2	0.05 cos 45° (1/3) + 0.20	= 0.21179
3	0.05 cos 45° (1/2) + 0.20	= 0.21768
4	0.24 (0.5)	= 0.12
5	0.25 cos 45° (1/3) + 0.07	= 0.128926
6	0.07 (0.5)	= 0.035
7	0.20 (0.5)	= 0.10

First moment of area:

Section No.		$A_i\bar{y}_i$ (in.^{3})
1	0.0002 (0.2388)	$= 4.776 \times 10^{-5}$
2	0.00625 (0.21179)	$= 1.32369 \times 10^{-4}$
3	0.001366 (0.21768)	$= 2.97351 \times 10^{-4}$
4	0.0192 (0.12)	= 0.002304
5	0.015625 (0.128926)	= 0.00201447
6	0.012374 (0.035)	$= 4.3309 \times 10^{-4}$
7	0.014798 (0.10)	= 0.0014798

Calculation of distance to neutral axis in Y direction from reference line:

$$\bar{Y} = \Sigma A_i\bar{y}_i/A_{total}$$

$$= 0.00670844/0.0641884$$

$$= 0.10451795 \text{ inch.}$$

For $\bar{X}$, the distance to neutral axis in X direction from a second reference line:

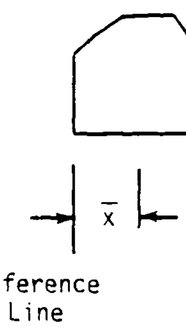

Distance to reference line for each section:

Section No.		$\bar{x}_i$ (in.)
1	2 (0.04 cos 15°)/3 + (0.05) sin 45°	= 0.061113522
2	2 (sin 45°)0.05/3	= 0.0235702
3	0.05 (sin 45°) + (0.04) cos 15°/2	= 0.0546739
4	0.5 (0.08) + sin 45° (0.05) + 0.04 (cos 15°)	= 0.1139924
5	0.08 + sin 45° (0.05) + cos 15° (0.04) + 0.25 (cos 45°)/3	= 0.212918
6	0.08 + sin 45° (0.05) + cos 15° (0.04) + 0.25 (cos 45°) 0.5	= 0.396374
7	0.5 (0.05 (cos 45°) + 0.04 (cos 15°))	= 0.0369963

First moment of area:

Section No.		$A_i x_i$ (in.^{3})
1	(0.0002) 0.61113522	= 1.2222704×10^{-5}
2	(0.000625) 0.0235702	= 1.4731375×10^{-5}
3	(0.001366) 0.0546739	= 7.468455×10^{-5}
4	(0.0192) 0.1139924	= 0.00218865
5	(0.015625) 0.212918	= 0.003326843
6	(0.012374) 0.396374	= 0.004904731
7	(0.014798) 0.0369963	= 5.47471×10^{-4}

Calculation of distance to neutral axis in X direction from reference line:

$$\overline{X} = \Sigma A_i \bar{x}_i / A_{total}$$

$$= 0.006780884/0.0641884$$

$$= 0.10451795 \text{ inch.}$$

DISTRIBUTION LIST

No. of Copies	To
1	Office of the Under Secretary of Defense for Research and Engineering, The Pentagon, Washington, DC 20301
	Metals and Ceramics Information Center, Battelle Columbus Laboratories, 505 King Avenue, Columbus, OH 43201
1	ATTN: Sharad Pednekar
	Commander, Defense Technical Information Center, Cameron Station, Bldg. 5, 5010 Duke Street, Alexandria VA 22304-6145
2	ATTN: DTIC-FDAC
	Commander, U.S. Army Materiel Command, 5001 Eisenhower Avenue, Alexandria, VA 22333
1	ATTN: AMCQA-P, S. J. Lorber
	Commander, Pacific Missile Test Center, Point Mugu, CA 93042
1	ATTN: Sam Keller, Code 2043
1	Steve Kohler, Code 2041
1	John Durda, Code 2041
1	Carl Louck, Code 2041
1	John Piercy, Code 2041
	Commander, U.S. Army Laboratory Command, 2800 Powder Mill Road, Adelphi, MD 20783-1145
1	ATTN: AMSLC-IM-TL
1	AMSLC-CT
	Commander, Rock Island Arsenal, Headquarters AMCCOM, Rock Island, IL 61299-6000
1	ATTN: AMSMC-PCA-WM, Joe Wells
1	AMSMC-QAM-I, Gary Smith
1	AMSMC-ASR-M, Brian Kunkel
	Commander, U.S. Army Test and Evaluation Command, Aberdeen Proving Ground, MD 21005
1	ATTN: Library
	Commander, U.S. Army Engineer School, Fort Belvoir, VA 22060
1	ATTN: Library
	Naval Air Systems Command, Department of the Navy, Washington, DC 20360
1	ATTN: AIR-03PAF
	Naval Research Laboratory, Washington, DC 20375
1	ATTN: Code 5830
	Naval Air Development Center, Warminster, PA 18974
1	ATTN: Library
	Director, U.S. Army Materials Technology Laboratory, Watertown, MA 02172-0001
2	ATTN: SLCMT-TML
2	Authors

U.S. Army Materials Technology Laboratory
Watertown, Massachusetts 02172-0001
FAILURE ANALYSIS OF A MISSILE
LOCKING HOOK FROM THE F-14 JET -
Victor K. Champagne, Jr. and Gary Wechsler

Technical Report MTL TR 89-90, September 1989, 54 pp-
illus-tables

AD__________
UNCLASSIFIED
UNLIMITED DISTRIBUTION

Key Words

High strength steels
Fatigue (mechanics)
Missile hook

A comprehensive metallurgical examination of the missile hook was conducted at the U.S. Army Materials Technology Laboratory (MTL) to determine the probable cause of failure. The component is one of two launcher housing support points for the Sparrow Missile and is located on the F-14 jet. The missile hook failed while in service. Chemical analysis verified that the part was fabricated from 300M steel. It was determined by metallographic examination that the microstructure was martensitic. Visual inspection and light optical microscopy of the load-bearing area showed that the surface coating "Microlube" had been completely worn away during service, allowing corrosion to take place. Extensive pitting was found on surface regions near the fracture. Further analysis of the "Microlube" coating revealed that required thickness specifications were exceeded. The machined radius where the fracture initiated was measured and found to be sharper than specified. The mechanical properties of the material compared favorably with requirements. Scanning electron microscopy (SEM) and energy dispersing spectroscopy (EDS) were used to characterize the fracture surface and the surface coatings. The entire manufacturing history of the missile hook was reviewed and the service conditions were analyzed. Finally, a mechanics analysis was conducted in order to calculate the operating stresses, the critical crack size, and the critical stress intensity factor (Kic) for the conditions observed. The failure was attributed to a fatigue crack that had initiated at the base of an undercut radius on the machined lip of the component.

U.S. Army Materials Technology Laboratory
Watertown, Massachusetts 02172-0001
FAILURE ANALYSIS OF A MISSILE
LOCKING HOOK FROM THE F-14 JET -
Victor K. Champagne, Jr. and Gary Wechsler

Technical Report MTL TR 89-90, September 1989, 54 pp-
illus-tables

AD__________
UNCLASSIFIED
UNLIMITED DISTRIBUTION

Key Words

High strength steels
Fatigue (mechanics)
Missile hook

A comprehensive metallurgical examination of the missile hook was conducted at the U.S. Army Materials Technology Laboratory (MTL) to determine the probable cause of failure. The component is one of two launcher housing support points for the Sparrow Missile and is located on the F-14 jet. The missile hook failed while in service. Chemical analysis verified that the part was fabricated from 300M steel. It was determined by metallographic examination that the microstructure was martensitic. Visual inspection and light optical microscopy of the load-bearing area showed that the surface coating "Microlube" had been completely worn away during service, allowing corrosion to take place. Extensive pitting was found on surface regions near the fracture. Further analysis of the "Microlube" coating revealed that required thickness specifications were exceeded. The machined radius where the fracture initiated was measured and found to be sharper than specified. The mechanical properties of the material compared favorably with requirements. Scanning electron microscopy (SEM) and energy dispersing spectroscopy (EDS) were used to characterize the fracture surface and the surface coatings. The entire manufacturing history of the missile hook was reviewed and the service conditions were analyzed. Finally, a mechanics analysis was conducted in order to calculate the operating stresses, the critical crack size, and the critical stress intensity factor (Kic) for the conditions observed. The failure was attributed to a fatigue crack that had initiated at the base of an undercut radius on the machined lip of the component.

U.S. Army Materials Technology Laboratory
Watertown, Massachusetts 02172-0001
FAILURE ANALYSIS OF A MISSILE
LOCKING HOOK FROM THE F-14 JET -
Victor K. Champagne, Jr. and Gary Wechsler

Technical Report MTL TR 89-90, September 1989, 54 pp-
illus-tables

AD__________
UNCLASSIFIED
UNLIMITED DISTRIBUTION

Key Words

High strength steels
Fatigue (mechanics)
Missile hook

A comprehensive metallurgical examination of the missile hook was conducted at the U.S. Army Materials Technology Laboratory (MTL) to determine the probable cause of failure. The component is one of two launcher housing support points for the Sparrow Missile and is located on the F-14 jet. The missile hook failed while in service. Chemical analysis verified that the part was fabricated from 300M steel. It was determined by metallographic examination that the microstructure was martensitic. Visual inspection and light optical microscopy of the load-bearing area showed that the surface coating "Microlube" had been completely worn away during service, allowing corrosion to take place. Extensive pitting was found on surface regions near the fracture. Further analysis of the "Microlube" coating revealed that required thickness specifications were exceeded. The machined radius where the fracture initiated was measured and found to be sharper than specified. The mechanical properties of the material compared favorably with requirements. Scanning electron microscopy (SEM) and energy dispersing spectroscopy (EDS) were used to characterize the fracture surface and the surface coatings. The entire manufacturing history of the missile hook was reviewed and the service conditions were analyzed. Finally, a mechanics analysis was conducted in order to calculate the operating stresses, the critical crack size, and the critical stress intensity factor (Kic) for the conditions observed. The failure was attributed to a fatigue crack that had initiated at the base of an undercut radius on the machined lip of the component.

U.S. Army Materials Technology Laboratory
Watertown, Massachusetts 02172-0001
FAILURE ANALYSIS OF A MISSILE
LOCKING HOOK FROM THE F-14 JET -
Victor K. Champagne, Jr. and Gary Wechsler

Technical Report MTL TR 89-90, September 1989, 54 pp-
illus-tables

AD__________
UNCLASSIFIED
UNLIMITED DISTRIBUTION

Key Words

High strength steels
Fatigue (mechanics)
Missile hook

A comprehensive metallurgical examination of the missile hook was conducted at the U.S. Army Materials Technology Laboratory (MTL) to determine the probable cause of failure. The component is one of two launcher housing support points for the Sparrow Missile and is located on the F-14 jet. The missile hook failed while in service. Chemical analysis verified that the part was fabricated from 300M steel. It was determined by metallographic examination that the microstructure was martensitic. Visual inspection and light optical microscopy of the load-bearing area showed that the surface coating "Microlube" had been completely worn away during service, allowing corrosion to take place. Extensive pitting was found on surface regions near the fracture. Further analysis of the "Microlube" coating revealed that required thickness specifications were exceeded. The machined radius where the fracture initiated was measured and found to be sharper than specified. The mechanical properties of the material compared favorably with requirements. Scanning electron microscopy (SEM) and energy dispersing spectroscopy (EDS) were used to characterize the fracture surface and the surface coatings. The entire manufacturing history of the missile hook was reviewed and the service conditions were analyzed. Finally, a mechanics analysis was conducted in order to calculate the operating stresses, the critical crack size, and the critical stress intensity factor (Kic) for the conditions observed. The failure was attributed to a fatigue crack that had initiated at the base of an undercut radius on the machined lip of the component.